The Thesis Committee for Ulises Ruiz Barba
Certifies that this is the approved version of the following Thesis:

Seismic Analysis of a Retrofitted Reinforced Concrete Building in Mexico City

APPROVED BY
SUPERVISING COMMITTEE:

_____
Juan Murcia-Delso, Supervisor

_____
Patricia Clayton

Seismic Analysis of a Retrofitted Reinforced Concrete Building in Mexico City

by

Ulises Ruiz Barba

Thesis

Presented to the Faculty of the Graduate School of

The University of Texas at Austin

in Partial Fulfillment

of the Requirements

for the Degree of

Master of Science in Engineering

The University of Texas at Austin

August 2019

Acknowledgements

First and foremost, I would like to thank my advisor, Dr. Juan Murcia-Delso, for his support and guidance over the last two years while working in his research team. The completion of this thesis is a result of his willingness to share his experience. I would also like to thank Dr. Patricia Clayton for taking the time to read this Thesis and whose teachings were important in its development process.

This was not a one-man work, I would like to acknowledge Dr. David Murià-Vila, Dr. Sergio Alcocer and Dr. Oriol Arnau from the research team of the Universidad Nacional Autónoma de México (UNAM), who provided information and insight vital to the project.

In my journey towards this degree, The University of Texas at Austin proved an ideal place to improve both professionally and personally. I am greatly thankful to all the faculty, staff and fellow students who were part of this experience.

My acknowledgement would be incomplete without thanking the people involved in the Fulbright program, both in the United States of America and Mexico, who gave me the unique opportunity to live in a country other than my own while studying the field I am passionate about.

Finally, I would like to thank the biggest source of strength to follow through on my goals: my family.

Abstract

Seismic Analysis of a Retrofitted Reinforced Concrete Building in Mexico City

Ulises Ruiz Barba, MSE

The University of Texas at Austin, 2019

Supervisor: Juan Murcia-Delso

This thesis presents a study on the dynamic characteristics and seismic performance of a retrofitted concrete building located in the soft soil area of Mexico City. The original structure consisted of reinforced concrete frames in two orthogonal directions. Damaged during an earthquake in 1979, the building was retrofitted by installing external steel braces in its transverse direction and reinforced concrete infill walls in its longitudinal direction. The retrofitted structure presented minor damage after the 1985 and 2017 earthquakes.

The structural response of the building and the effectiveness of the retrofit has been assessed using an analytical model of the structure, in combination with data from post-earthquake damage inspections and ambient vibration tests. A three-dimensional linear elastic model of the building has been developed to study the modal characteristics of the building and its seismic response during the 1985 and 2017 events. The results of the analyses have been used to discuss the effects of the retrofit intervention, as well as the influence of the soil-structure interaction and other modeling assumptions in the response of the building.

Table of Contents

List of Tables

List of Figures

Chapter 1: Introduction

1.1: BACKGROUND

Mexico City has a long history of seismic activity with the most severe earthquakes in recent history occurring in 1979, 1985 and 2017. In March 1979 a 7.4-magnitude earthquake resulted in the collapse of the Universidad Iberoamericana (Fig 1.1) and the loss of electrical power in 20% of the Mexican territory (El Pais, 1979). While the material losses were high, only five people lost their lives during the event.

Figure 1.1: Photo of the collapsed buildings from the Universidad Iberoamericana (IBEROMX, 2017)

In contrast, the 8.1-magnitude 1985 Mexico City earthquake caused over 10,000 deaths and resulted in collapse and damage of modern construction that had not been seen before (Fig. 1.2). In the months and years following this earthquake, there was an unparalleled effort to repair and retrofit concrete buildings.

Figure 1.2: Collapsed building in Tlatelolco after the 1985 earthquake (BBC, 2017)

On September 19, 2017, a 7.1-magnitude intraslab earthquake struck Central Mexico. The earthquake caused 369 deaths, 228 of them in Mexico City, and damaged thousands of buildings. Thirty-eight buildings collapsed and several dozens were severely damaged in Mexico City (Fig 1.3).

Figure 1.3: Building in Viaducto Aleman: Google street view before the 2017 earthquake (left), collapsed building after the event (right) (The Huffpost, 2017)

A particular aspect of the seismic hazard in Mexico City is the local soil conditions which are unique in the world. Built on an ancient lakebed (Fig 1.4), the soft clay layer can reach depths of more than 70 m (~230 ft) in some areas of the city having an amplifying effect on the seismic waves that reach the city. As a result, site effects and soil-structure interaction play a significant role in the seismic response of buildings in Mexico City.

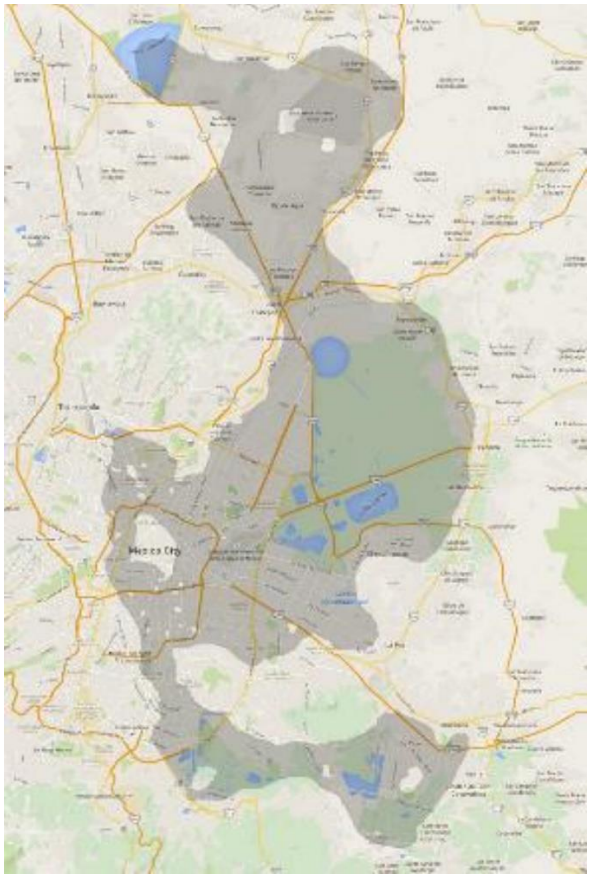

Figure 1.4: Location of the former lake Texcoco over a map of today's Mexico City (ATLATD, 2019)

1.2: MOTIVATION AND OBJECTIVES

The September 19, 2017 earthquake represented the first severe test for many concrete buildings that were retrofitted in prior years, namely in 1979 but mainly in 1985. The study of the performance of these retrofitted buildings can provide unprecedented evidence about the effectiveness of rehabilitation methods, which can contribute to extract valuable lessons to improve disaster resilience.

This MS thesis presents an analytical study on the dynamic properties and seismic response of the Durango building, which was retrofitted after being damaged during the 1979 earthquake. The Durango building had previously been studied by Downs et al. (1991) after the 1985 earthquake combining force-vibration tests and linear elastic analysis. After the 2017 event, a research team from the University of Texas at Austin and Universidad Nacional Autónoma de México (UNAM) inspected the building and the UNAM team also conducted ambient vibration tests.

The availability of reliable information and previous data on the building made it a perfect object of study. Moreover, the location of the building in an area where the damage of the 2017 earthquake was concentrated added to the reason to conduct this analysis. This is highlighted in Figure 1.5, which shows that one-third of the collapses (13) were within a 3 km (1.86 miles) radius and 6 within a 1.6 km (1 mile) radius.

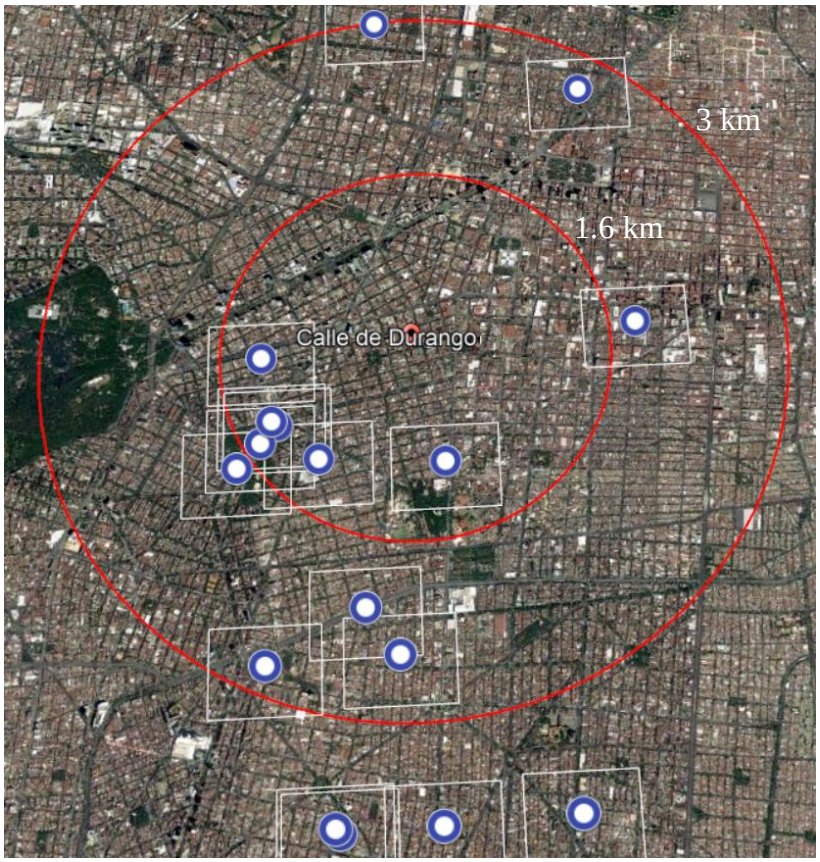

Figure 1.5: Location of the Durango building relative to collapses during the 2017 earthquake

The goal of this thesis is to conduct a detailed assessment of the seismic response of the Durango building, a retrofitted concrete structure, during the 2017 event combining results from ambient vibration tests and analytical methods, namely modal and time-history dynamic analyses. Such analyses are ultimately intended to study the effectiveness of the retrofits applied to this building.

1.3: STRUCTURE OF THE THESIS

Chapter 2 of this thesis presents a description of the characteristics and past earthquake performance of the Durango building, with emphasis on those aspects that are necessary for the accurate development of the analytical model. This chapter also includes an overview of the previous studies on the building as well as results from vibration tests conducted on the building to assess its dynamic properties.

Chapter 3 describes the computer model developed to analytically study the response of the building. This description includes the main modeling assumptions in terms of material properties, section properties, element connectivity, mass/weight distribution, and soil-structure interaction.

Chapter 4 presents results from modal analyses of the building using the computer model and compares them to vibration test results. This chapter also includes results of a sensitivity study conducted to calibrate and validate building modeling assumptions.

Chapter 5 presents results from linear elastic time-history analyses conducted with the computer model using records from the 1985 and 2017 earthquakes. These analyses are used to characterize the response of the building in these two events and assess the effectiveness of the retrofit methods applied in the building.

Chapter 6 summarizes the main findings and conclusions of this study and presents recommendations for future research.

Chapter 2: Building Description and Background

2.1: ORIGINAL PROJECT

The Durango building, built in 1972, has 12 stories with a basement and a penthouse to access the roof. The original structure consists of RC frames in two orthogonal directions as shown in Fig. 2.1. The building plan measures 11.9 m (~39 ft) by 20.9 m (~68.5 ft) and the typical story height is 3.05 m (10 ft). The lateral forces were originally resisted by Frames 1 through 5 in the east-west (E-W) direction, while Frames A and C resisted lateral forces in the north-south (N-S) direction. Frames 1 and 5 are characterized by single-span deep spandrels that are part of the façade (Fig. 2.2). The exception is Frame 1 at PB level where the spandrel is eliminated to provide access to the parking. Frames 2 through 4 are identical and consist of 3 columns and haunched beams as shown in Fig. 2.3. In the N-S direction, Frames A and C are identical, while Frame B has the exterior column omitted. It can be considered that Frame B does not participate in the lateral load-carrying system given that column-slab connections are not prepared to transfer the moment.

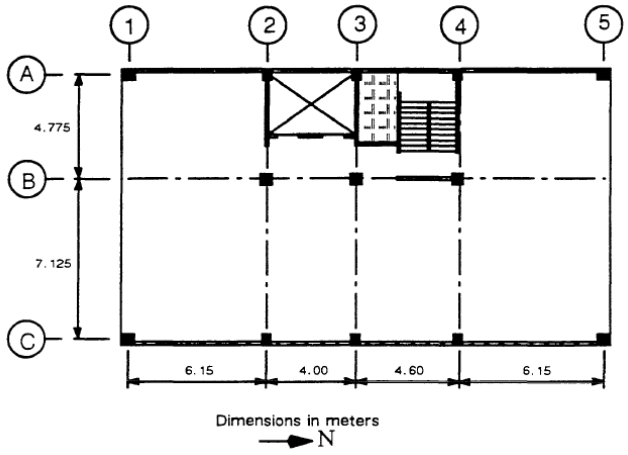

Figure 2.1: Typical floor plan for the Durango building (Downs, et al., 1991)

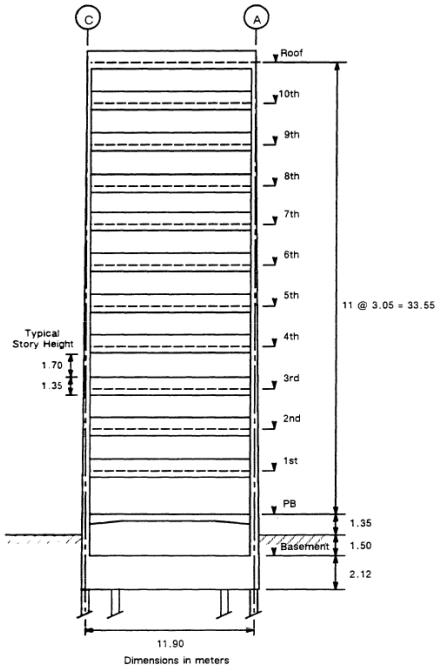

Figure 2.2: Elevation of Frame 5 of the building prior to retrofit (Downs, et al., 1991)

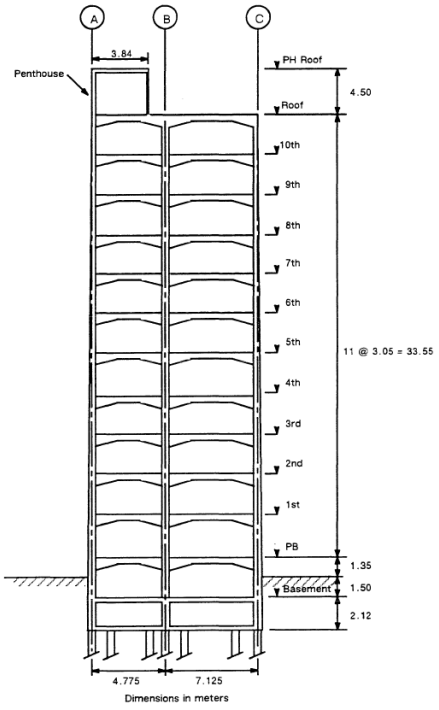

Figure 2.3: Elevation of Frame 2, 3 and 4 of the building (Downs, et al., 1991)

Other major characteristics of the structure include the tapered columns throughout the height of the building. Exterior columns of Frames 1 through 5 are tapered continuously, while interior columns of Frames 2 through 4 are tapered in steps (Fig 2.4). Typical column sections are shown in Figure 2.5 with additional information about the column dimensions and reinforcement provided in Downs et. al (1991).

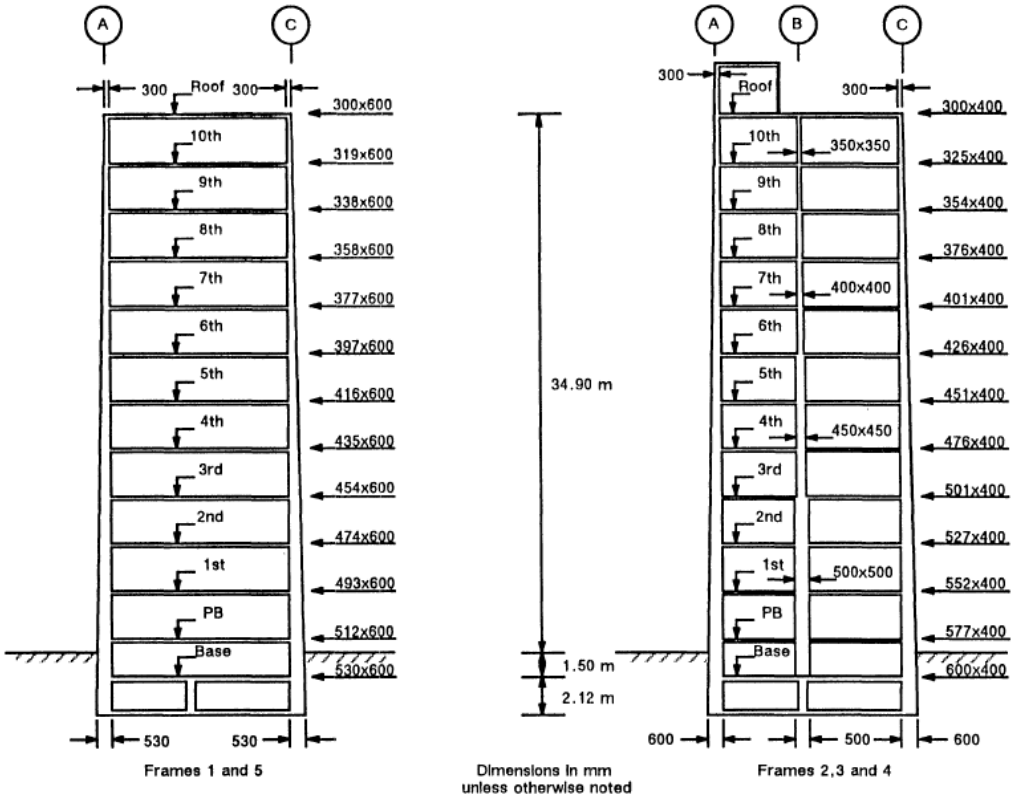

Figure 2.4: Schematic diagrams showing column tapering (Downs, et al., 1991)

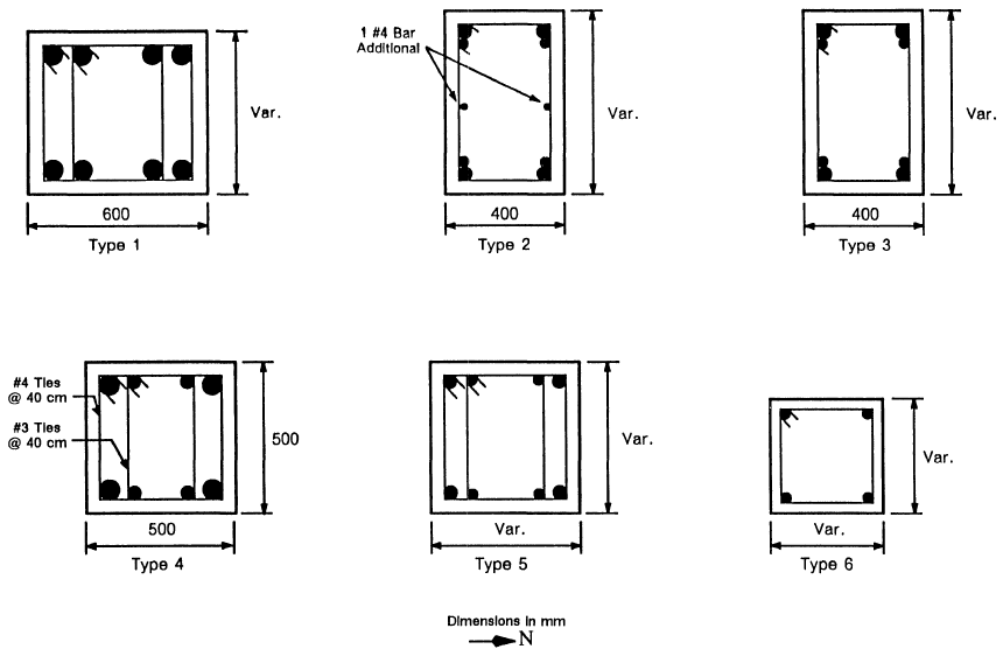

Figure 2.5: Column cross-sectional types (Downs, et al., 1991)

The floor system consists of a concrete slab with one-way joists running in the N-S direction as shown in Fig 2.6. The slab is 50 mm (~2 in) thick, and the joists (Fig. 2.7) measure 300 mm (~11.8 in) in depth and have a web of 100 mm (~3.9 in). These joists are supported by two types of beams running E-W: deep spandrels in Frames 1 and 5 (Fig. 2.8) and haunched beams for Frames 2 through 4 (Fig 2.9). Only Frames A and C have beams in the N-S direction, the details of these edge beams are shown in Fig 2.10. More details on the floor system design are provided in Downs et al. (1991).

Infill walls in both longitudinal (N-S) façades were constructed using red clay bricks. These walls are 150 mm (~5.9 in) in thickness and were isolated from the main structure using gaps filled with Celotex plates on the sides and top.

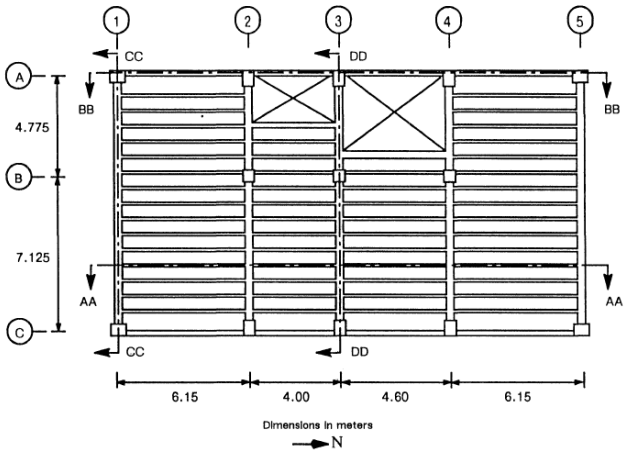

Figure 2.6: Plan view of floor system (Downs, et al., 1991)

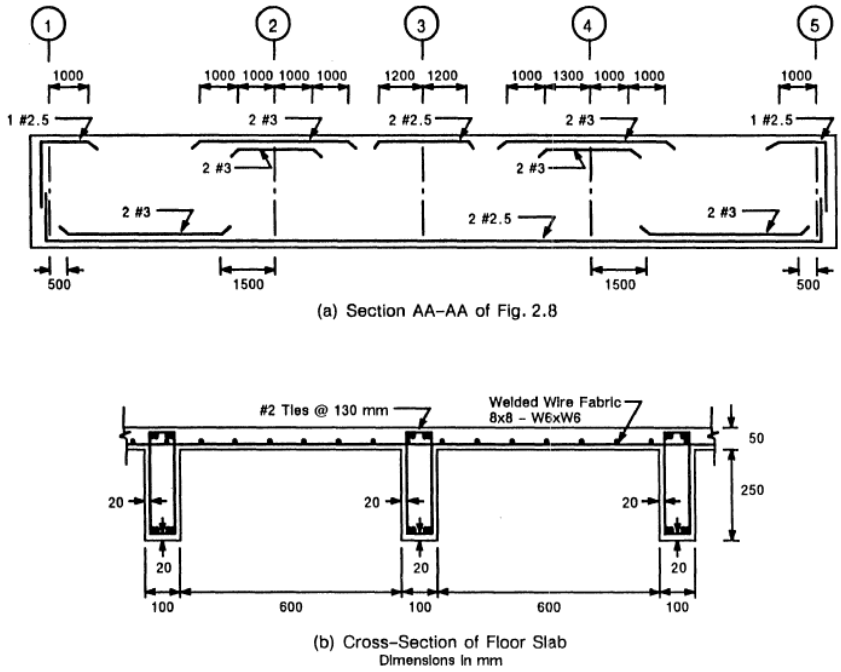

Figure 2.7: Details of typical floor joist (Downs, et al., 1991)

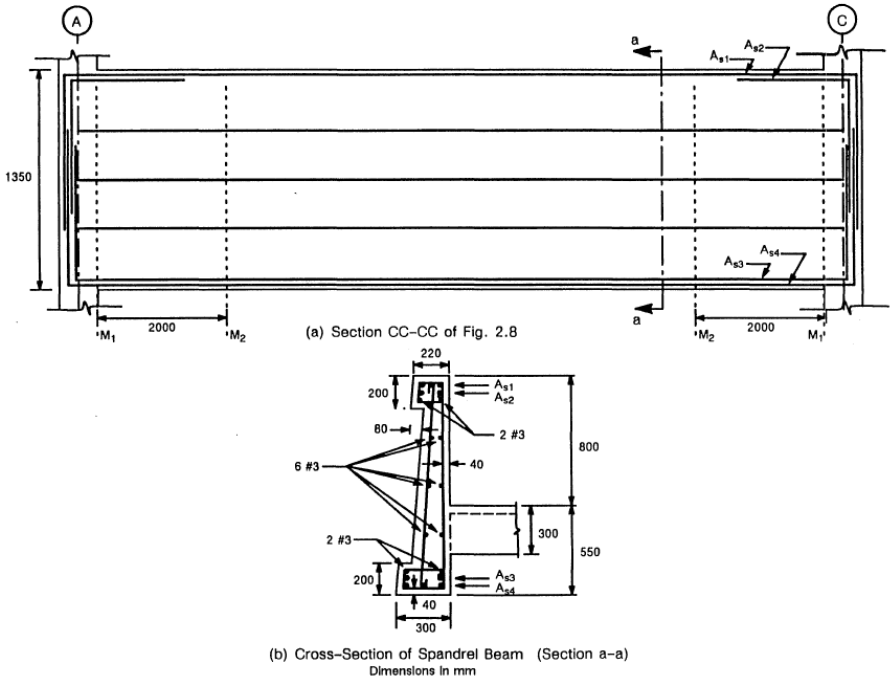

Figure 2.8: Details of spandrel beam (Downs, et al., 1991)

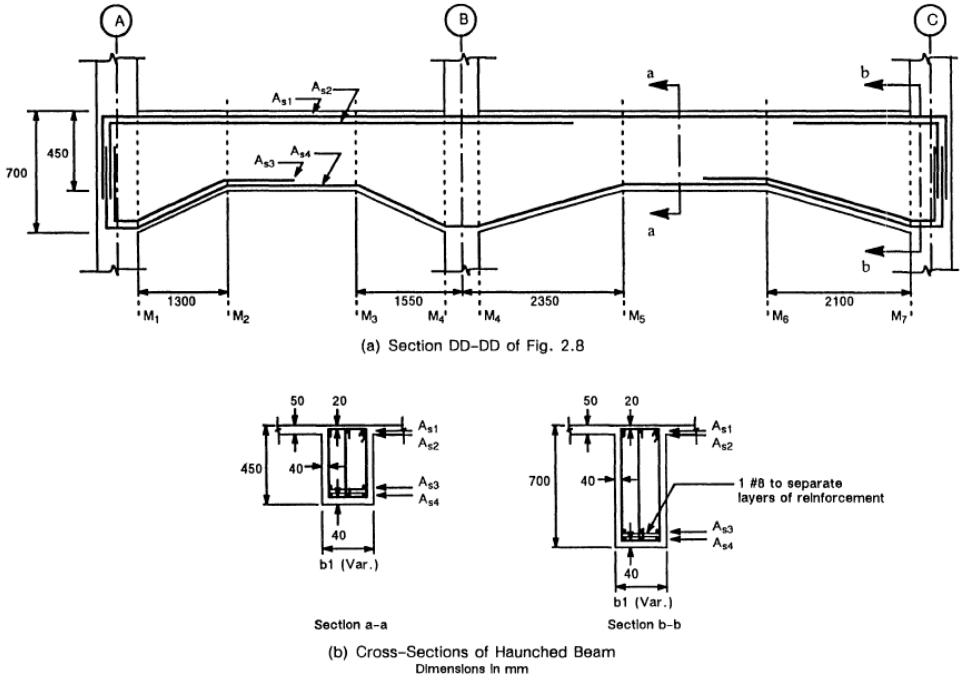

Figure 2.9: Details of haunched beam (Downs, et al., 1991)

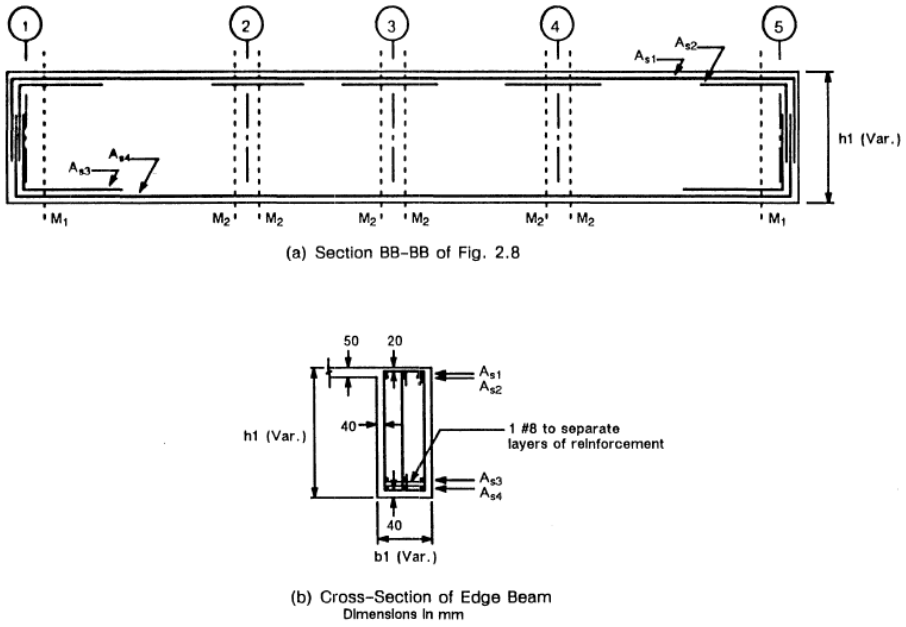

Figure 2.10: Details of edge beam (Downs, et al., 1991)

The foundation of the building consists of a voided mat 2.12 m (~7 ft) thick with rib beams running along the column lines. These ribs are 400 mm (~15.7 in) in width and are connected to a 300 mm (~11.8 in) thick foundation slab at the bottom and a 120 mm (~4.7 in) thick basement slab at the top making a rigid foundation (Fig 2.11). The mat is supported by 42 concrete piles measuring 450 mm (~17.7 in) in diameter and 25 m (~82 ft) in length.

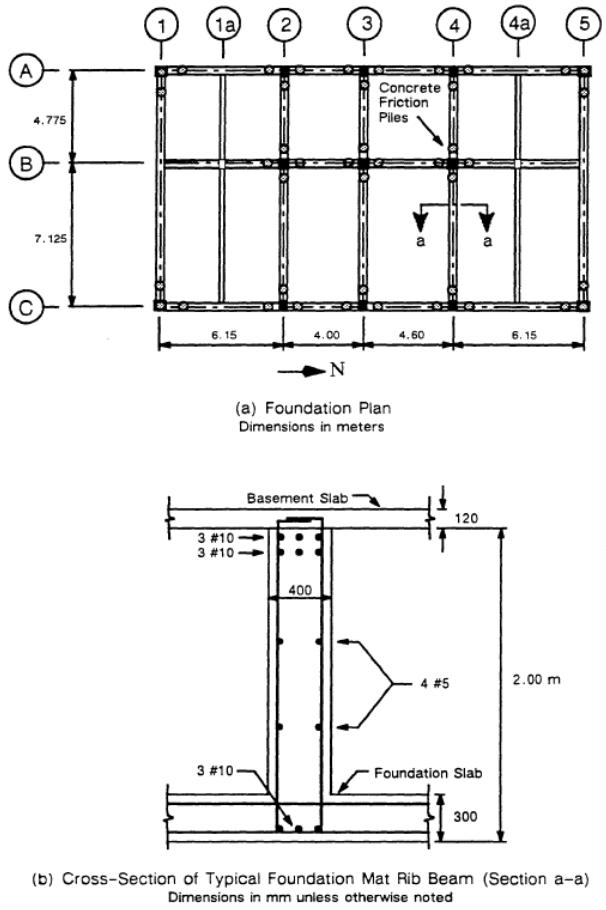

Figure 2.11: Original foundation of the Durango building (Downs, et al., 1991)

2.2: 1979 EARTHQUAKE

The Durango building suffered damage from a 7.6 magnitude earthquake on March 14, 1979. The damage was concentrated in stories 1 through 3 and was caused by the E-W (transverse) shaking of the building. The exterior frames (1 and 5) suffered from cracking and spalling of the beam-column connection in these levels (Fig. 2.12). Additionally, the deep spandrels experienced diagonal cracking over most of its length due to shear and flexural effects. Most of the columns had some degree of cracking in the lower

level but column B-3 also experienced crushing. This was later attributed to construction problems rather than a deficient seismic design (Downs, et al., 1991).

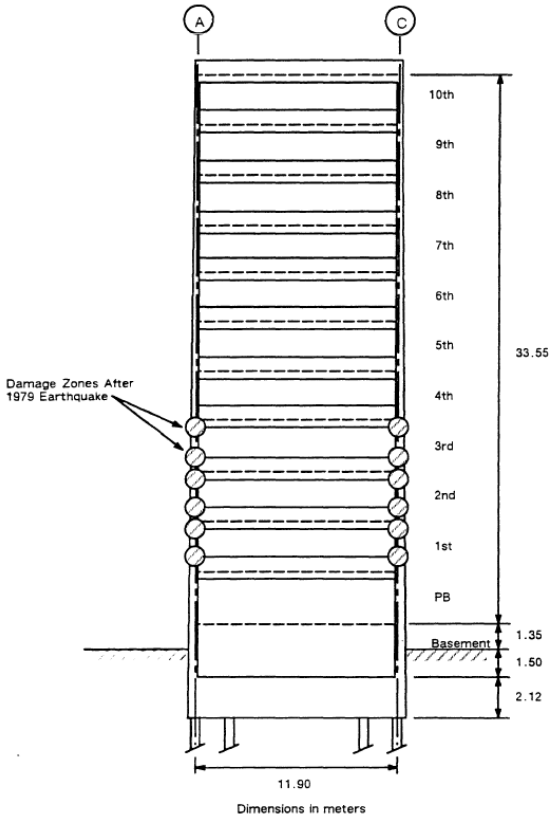

Figure 2.12: Damage zones of Frame 1 after the 1979 earthquake (Downs, et al., 1991)

The reason for the concentration of the damage in these areas is most likely the higher stiffness of Frames 1 and 5. This due to the short column effect, caused by the deep spandrels, which was not accounted for given the available tools and standard procedures at the time of design (Downs, et al., 1991). The result was an increase of the forces resisted during an earthquake and the concentration of these forces in these two frames, given their higher stiffness when compared to Frames 2 through 4.

2.3: BUILDING RETROFIT AND POST-RETROFIT PERFORMANCE

2.3.1: 1979 Retrofit

Following the earthquake, the structural engineer Enrique del Valle was hired to retrofit the building. His final proposal consisted of an external steel braced frame to resist the transverse (E-W) forces and RC infill walls in the longitudinal direction.

Damaged elements of the existing structure were repaired before the retrofit systems were installed. Cracks were filled with epoxy, and a steel jacket was added to the columns of Frames 1 and 5 up to the 4th story. The jacket consisted of 1/2" A36 steel plates welded together to form a box around the column. Additionally, #8 rebars were welded in the interior of the plates, and the voids between the plates and the previously chipped column were filled with expansive mortar. All this to improve the bond between the jacket and the existing structure.

As mentioned above, the retrofit included a new steel frame added to both façade Frames (1 and 5). The frame elevation is presented in Fig. 2.13, while the extension to the foundation is shown in Fig. 2.14. The built-up box columns of these steel frames, through the 4th story, and the diagonal bracing at the 1st level were fabricated with 5/8" A36 steel plates. The rest of the columns use 1/2" A36 plates. The rest of the diagonal bracing consisted of two channels welded together forming a box. These were later connected to the structure using gusset and stitch plates. Two C8x11.5 A36 channels were used up to the 7th story, while two C6x8.2 A36 channels are used in the rest of the stories. The extension to the foundation consisted of footings measuring 3.53 m (~11.6 ft) x 1.50 m (~4.9 ft) and 2.64 m (~8.7 ft) in depth. Each footing is connected to three steel piles of 77 mm (3 in) in diameter and 25 m (~82 ft) in length. To properly attach the steel frame to the

existing concrete structure the floor system was reinforced midspan as shown in Figure 2.15. In the corners connections as the ones presented in Figure 2.16 were added.

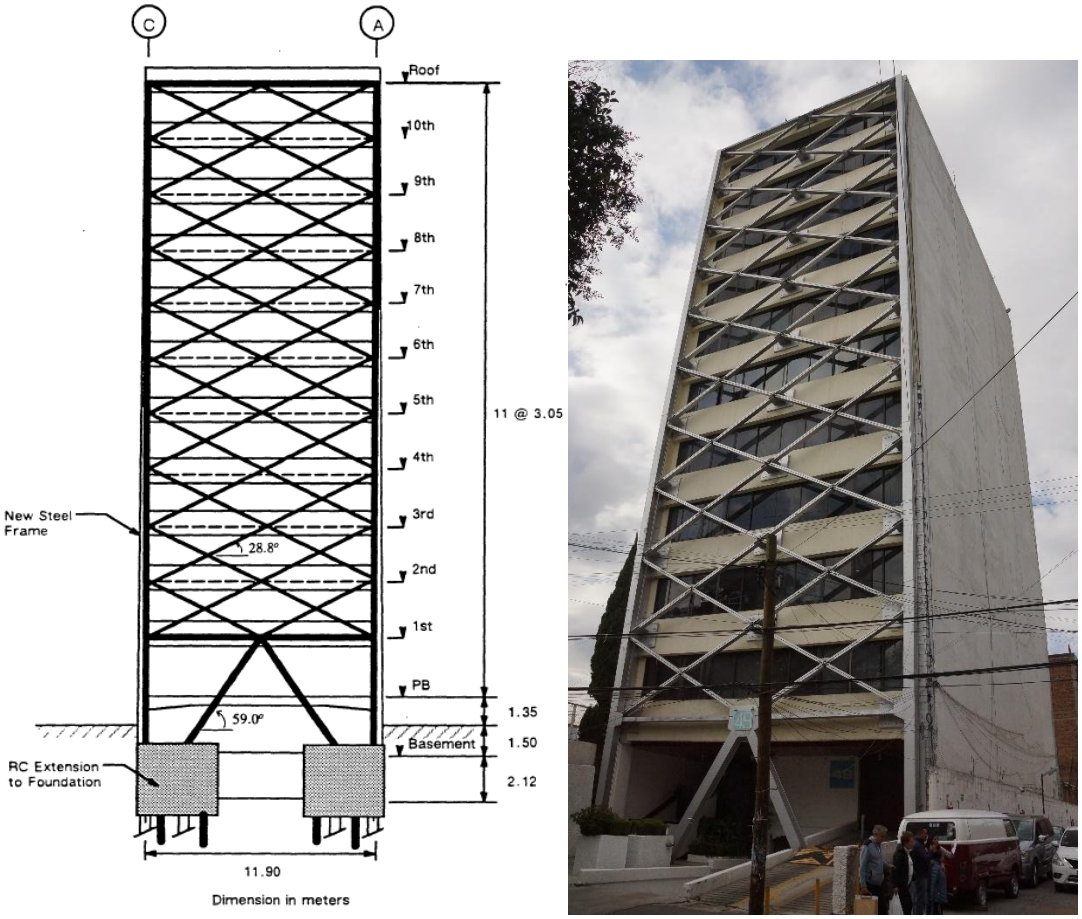

Figure 2.13: Elevation of Frame 5 after retrofit (Downs, et al., 1991) alongside a view of the southeast corner of the building

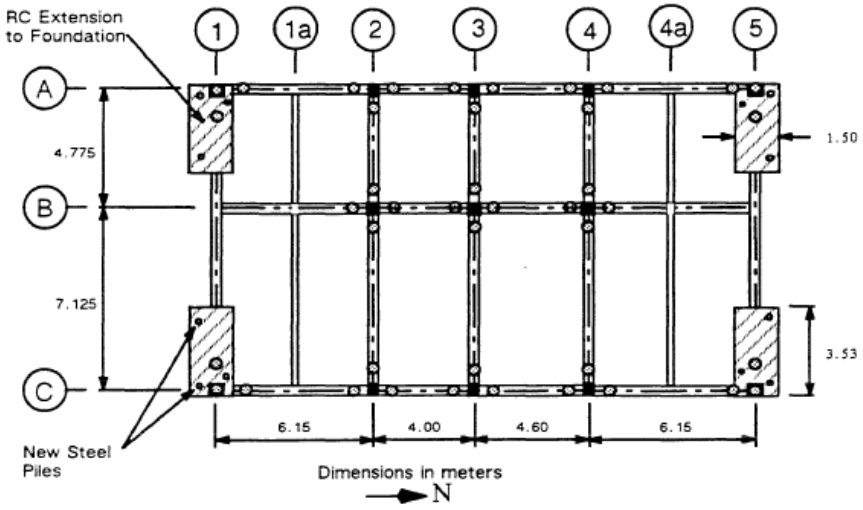

Figure 2.14: Foundation plan depicting retrofit elements (Downs, et al., 1991)

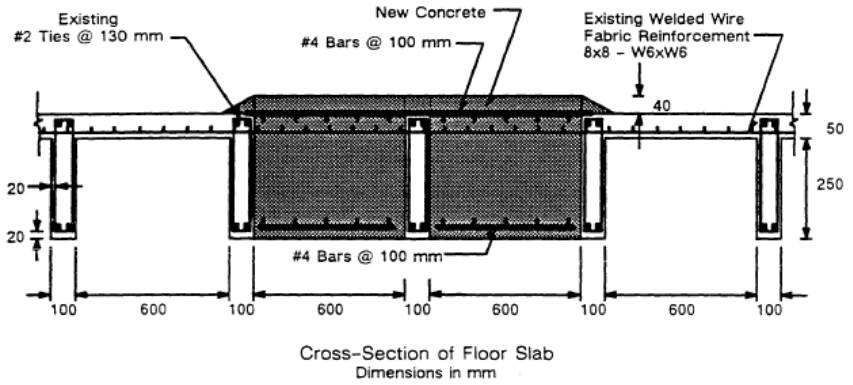

Figure 2.15: Detail of typical slab reinforcement at locations of steel frame attachment to Frames 1 and 5 (Downs, et al., 1991)

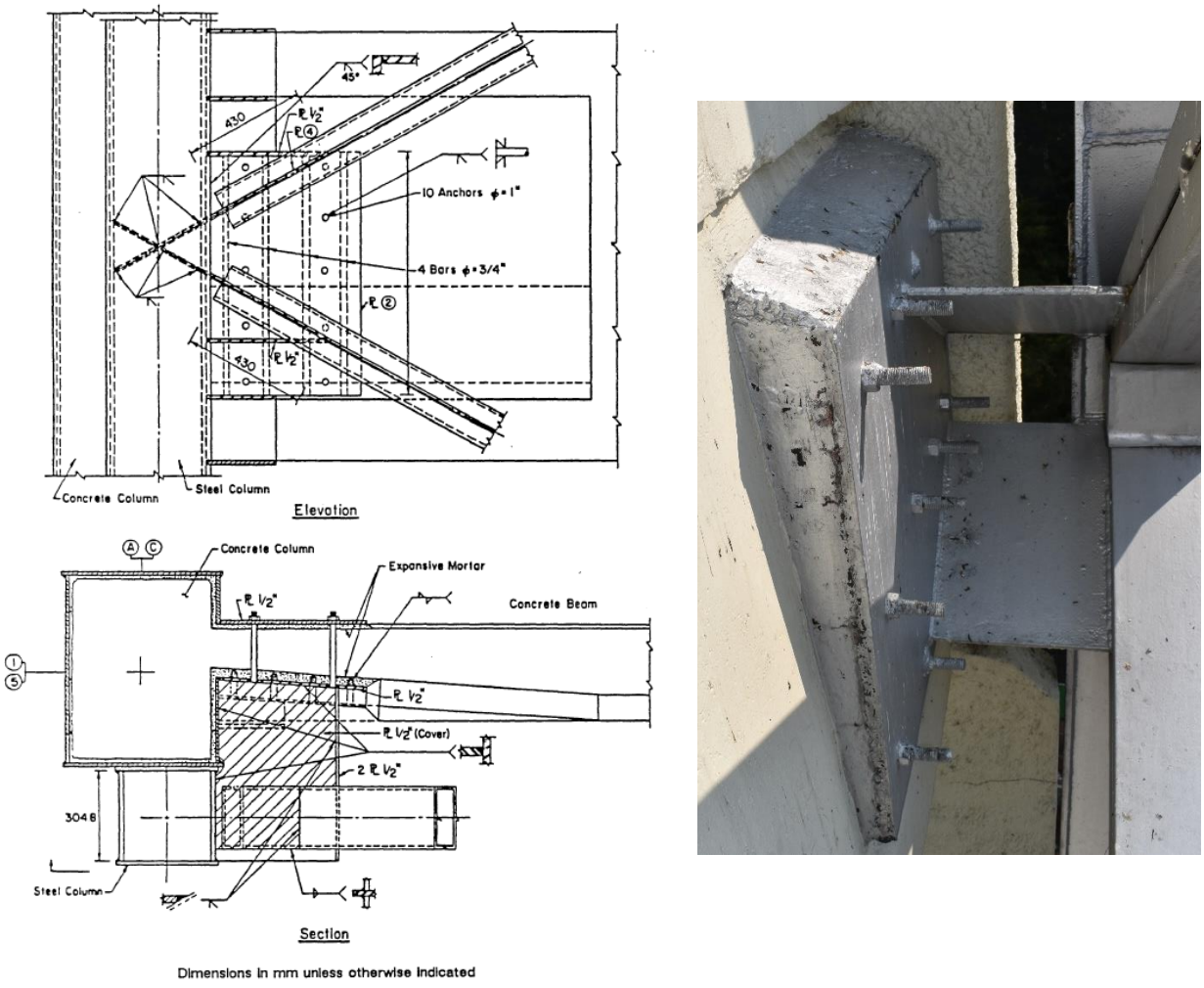

Figure 2.16: Typical detail for attachment of new steel frame to existing concrete frame (Downs, et al., 1991) alongside a view of the connection

RC infill walls were added to bays 1-2 and 4-5 of Frames A and C to strengthen the longitudinal direction (N-S) as shown in Fig. 2.17. These infills, measuring 60 mm (~2.4 in) in thickness, were connected to the existing masonry infills, columns and beams using nails, while the Celotex was removed and the gap filled with mortar (Fig. 2.18). The vertical and horizontal reinforcement ratios of the RC infill walls were 1.27% in stories 1-4, 0.64% in stories 5-7, and 0.42% in stories 8-10. While no information is reported about

interventions in the masonry infills of bays 2-3 and 3-4, it has been assumed that the Celotex was also removed in these bays and the gap was filled with mortar. This assumption has been verified during the calibration of the model as described in Chapter 4.

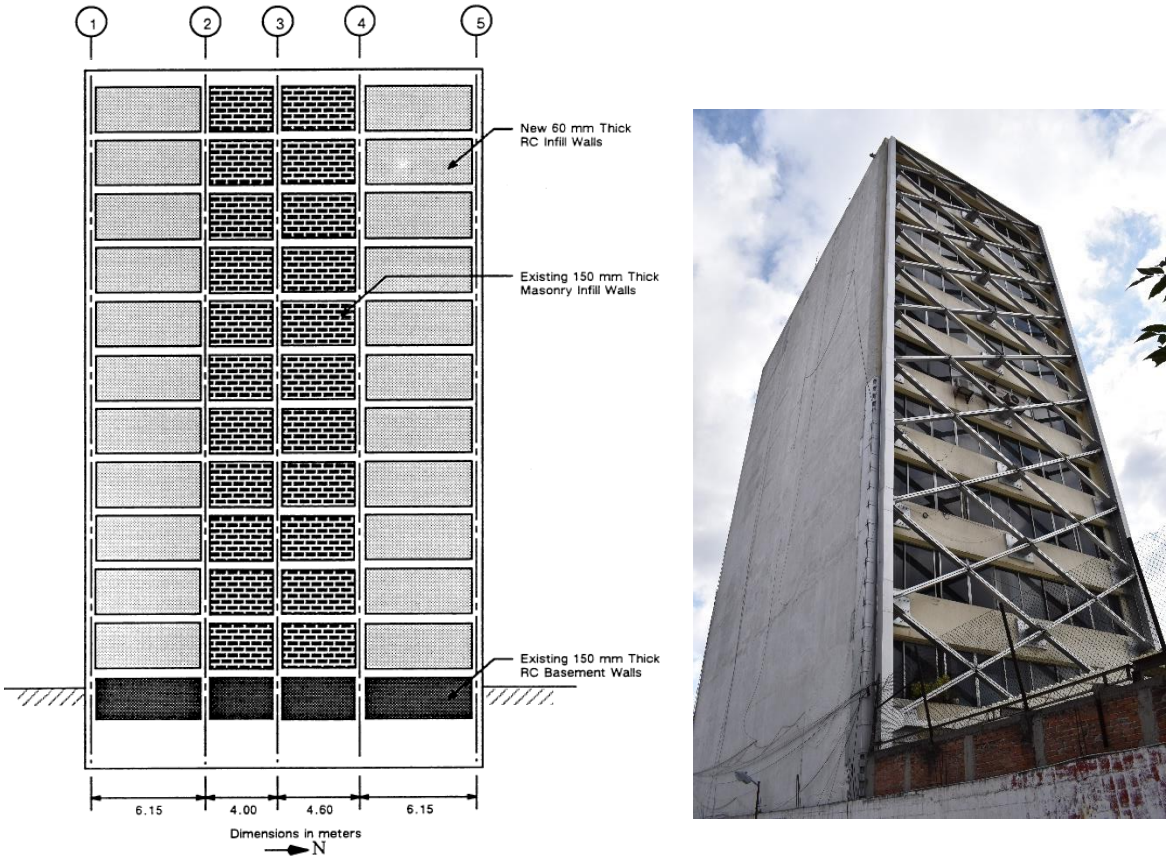

Figure 2.17: Elevation of Frame C showing new RC infill walls (Downs, et al., 1991) alongside a photo of the southeast corner of the building

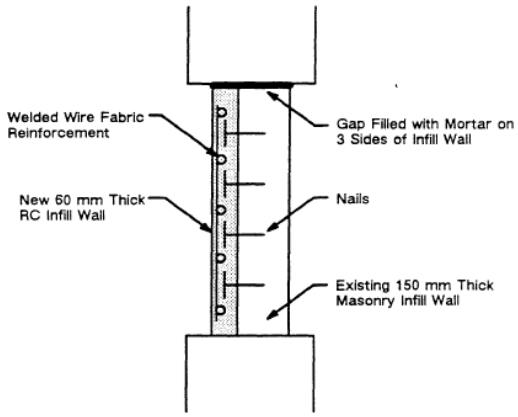

Figure 2.18: Wall reinforcement detail (Downs, et al., 1991)

The structural retrofit intervention was designed in accordance with the Mexico City code (1976). A conservative approach was used with a ductility factor of 2 instead of the 4 allowed by the code, and the steel frame was assumed to resist the entirety of the transverse shear (Del Valle, 1980)

2.3.2: 1985, 2012 and 2017 Earthquakes

After the retrofit, the building has been subjected to three major earthquakes. The first one being the 19 September 1985 with a magnitude of 8.1. During this event, the building suffered no visible damage with only slight cracking in the new RC infill walls according to Downs et al. (1991).

The second major event was a 7.4 magnitude earthquake on March 20, 2012. No damage reports were made, but some of the steel jacketing welds may have cracked given that they were later repaired according to the building administration.

On September 19, 2017, struck the most recent earthquake. It had a 7.1 magnitude and an epicenter located 120 Km (~74.5 miles) away from Mexico City causing the collapse of 38 buildings. The Durango building presented minor damage after the

earthquake. Inclined cracks were observed in the spandrel beams at the connection with the steel bracing (Fig. 2.19). A few connections also showed loosened bolts and gaps between the steel plate and the spandrel (Fig. 2.19a). However, it is possible that those damages were previous to this earthquake. The building was also reported to lean 231 mm (~9.1 in) or 0.006% of the height of the building in the E-W direction and 150 mm (~5.9 in) or 0.004% of the height of the building in the N-S direction after the earthquake.

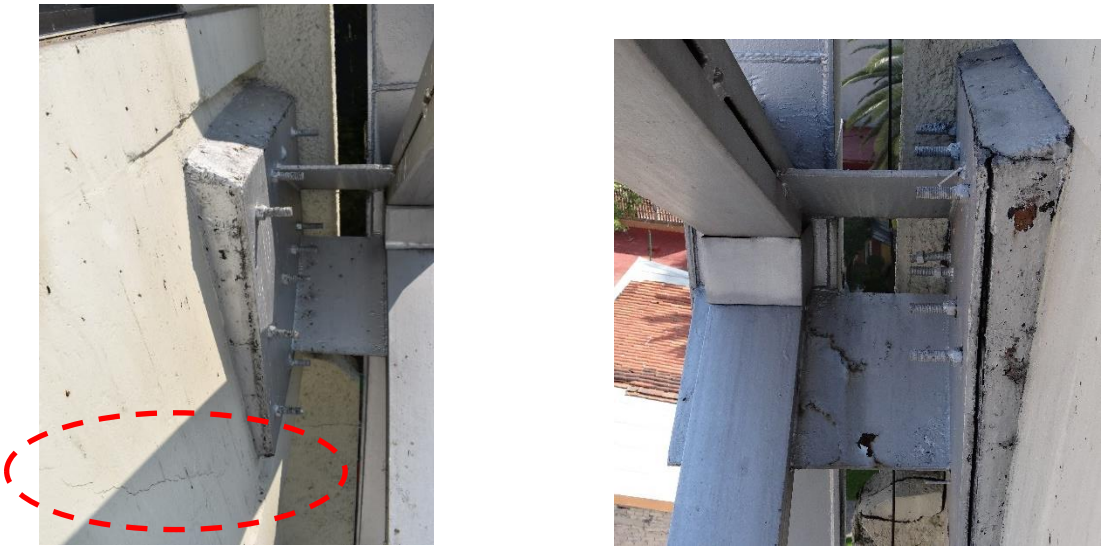

Figure 2.19: Cracking of spandrel beam at the connection with the steel frame (left) and loosened bolts and gap in connection between RC and steel frame (right)

As a result of the building leaning and shaking, elements of the parking structure were damage due to the lack of gap. Other non-structural damages were observed, such as the cracking in walls partition and the stairway walls (Fig 2.20).

Figure 2.20: Steel frame footing with the damage to adjacent parking structure (left) and crack in partition walls (right)

2.4: PREVIOUS STUDIES ON THE BUILDING

A study of the building was conducted by Foutch (1989) and Downs et al. (1991) after the 1985 earthquake. This study evaluated the retrofit scheme combining post-earthquake damage observations in 1979 and 1985, forced-vibration tests (FVT) conducted in 1987, and linear elastic analysis of the building. Additionally, Downs et al. (1991) report that ambient vibrations tests (AVT) were conducted before and immediately after the building retrofit in 1979. After the September 19, 2017 earthquake another ambient vibration test was conducted by Dr. David Murià-Vila and his collaborators at the Instituto de Ingeniería of the Universidad Nacional Autónoma de México (UNAM).

2.4.1: 1979 and 1987 Vibration Tests

As described in a report by Downs et al. (1991), ambient vibration tests were conducted prior to and after the retrofit. The measured fundamental E-W frequencies of the building were 0.535 Hz (T=1.86 seconds) before retrofit and 0.875 Hz (T=1.14 seconds) following retrofit, which indicates that the steel bracing increased the transverse stiffness of the structure significantly.

In January 1987 forced vibration tests were conducted in the building. The natural frequencies obtained from these tests are presented in Table 2.1. The tests showed a decrease in the natural E-W frequency from 0.875 Hz to 0.795 Hz. This reduction indicated a change in transversal stiffness sometime between the completion of the retrofit (early 1980) and these later tests. Possible explanations for this are provided in the report by Downs et al. (1991) such as indiscernible structural damage during the 1985 earthquake, nonstructural damage, softening of the soil and testing errors. The fundamental frequency in the longitudinal direction (NS) was 1.01 Hz.

Along with the frequencies, damping values and frequency ratios were obtained. The N-S direction presents a damping value of 4.8% which is close to the 5% typically implicit in the code-specified earthquake forces and design spectrum (Chopra, 2012). However, the E-W direction shows a 2.7% damping value which suggests that the steel frames dominate structural response in this direction (Downs, et al., 1991). The ratios between the first and second mode were 4.5 in the EW direction and 4.7 in the N-S direction.

Regarding the soil-structure interaction Downs et al. (1991) explains that the relative percentages of roof motion attributable to base translation and rocking are considerable. For the fundamental E-W mode shape, the average base translation contributes 4.2% of the measured roof translation and the average roof displacement caused by base rotation contributes 46%. For the fundamental N-S mode shape, the average base translation contributes 6.7% of the measured roof translation and the average roof displacement caused by base rotation contributes 49%. These are consistent with a very stiff structure supported by soft soil.

2.4.2: 2017 Ambient Vibration Test

An ambient vibration test of the building was conducted a few weeks after the earthquake of September 19, 2017, to characterize the vibration properties of the building. The team, led by Dr. Murià-Vila, obtained the vibration frequencies presented in Table 2.1. As shown, the fundamental frequencies are 0.85 Hz in the E-W direction and 1.17 Hz in the N-S with ratios, between the second and first modes of 4.2 and 4.5 respectively. These values are similar to those obtained from force vibrations in 1987 but the measurements indicate the natural frequencies of the building have slightly increased. This could be potentially caused by the soil-structure interaction and the reduction over time of the dominant site period as a result of the exploitation of the underground aquifers. The test also showed that more than 50% of the roof displacement was caused by base translation and rotation in both the E-W and N-S directions, which is consistent with the findings of the previous research.

The ratio of natural frequencies of vibration in a given direction of the building is an indicator of the type of response of a building. This ratio is related to the relative flexural stiffness between columns and beams, which is defined by the following ratio:

$$\rho = \frac{\sum EI_{beam}/L_{beam}}{\sum EI_{column}/L_{column}} \qquad (Eq.\ 2.1)$$

The behavior of a frame structure can range from one with fully restricted joint rotation (shear cantilever, $\rho = \infty$) to one with no restriction (flexural cantilever, $\rho = 0$) as shown in Fig 2.21. The relationship between ρ and the frequency ratios is described for a five-story frame in Figure 2.22, where f_1/f_2 or ω_1/ω_2 values range from ~3 and ~6.5 for a shear and a flexural cantilever respectively.

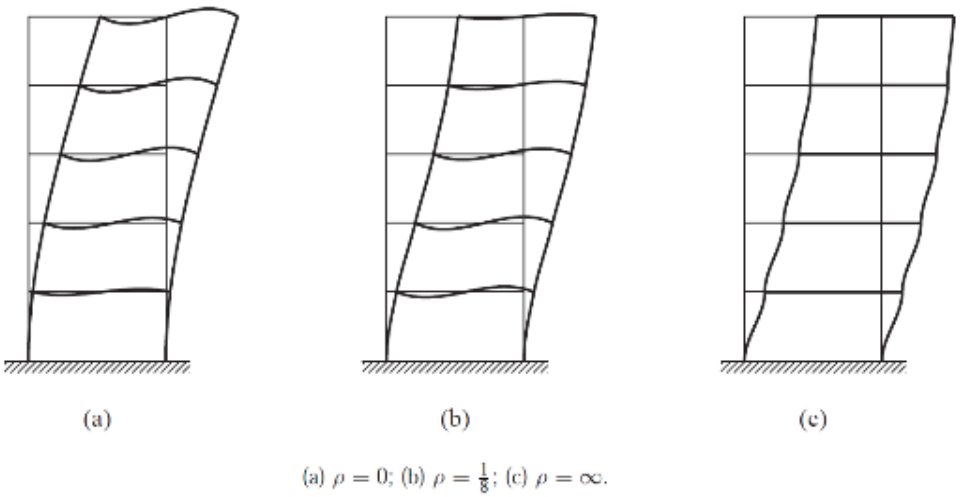

Figure 2.21: Example of deflected five-story buildings with different beam to column stiffness ratio (Chopra, 2012)

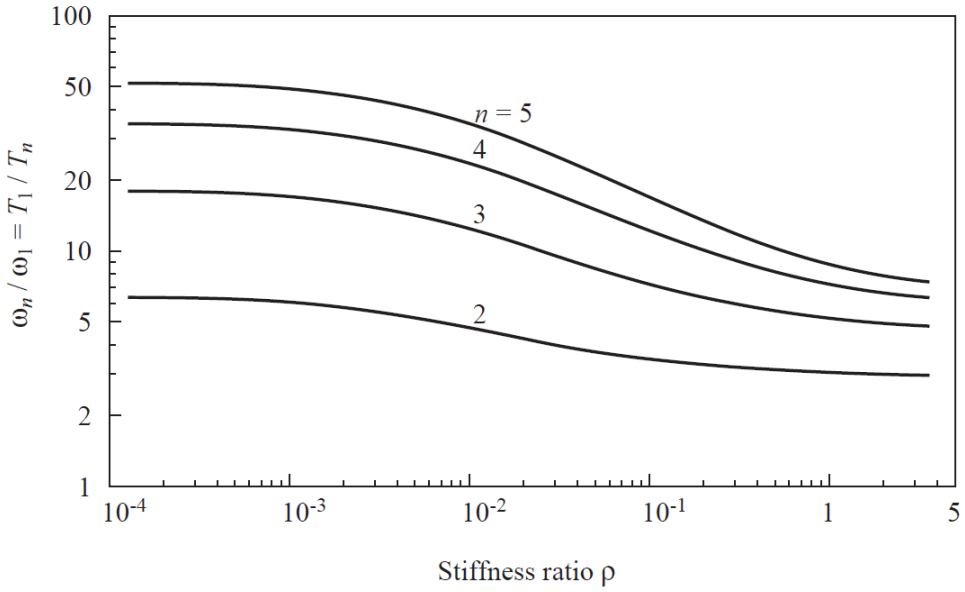

Figure 2.22: Natural vibration period ratios vs. beam-column stiffness ratio for a five-story frame (Chopra, 2012)

The dynamic properties of the Durango building obtained in 1987 and 2017, which are summarized in Table 2.1, presented ratios of 4.5 and 4.7 for E-W and N-S direction

respectively. This value indicates that the behavior presents an intermediate flexural/shear beam behavior. While the concrete frame alone would present a behavior closer to a pure shear beam, the retrofit elements (steel braces, RC infills) and soil flexibility contribute toward a flexural beam behavior. This aspect is further discussed using results of modal analysis in Chapter 4.

Table 2.1: Experimental dynamic properties of the building obtained from 1987 and 2017 vibration tests

Direction		1987 FVT	2017 AVT
E-W	f_1 [Hz]	**0.8**	**0.85**
	f_2 [Hz]	3.57	3.59
	f_2/f_1	4.5	4.2
N-S	f_1 [Hz]	**1.01**	**1.17**
	f_2 [Hz]	4.7	5.27
	f_2/f_1	4.7	4.5
Torsional	f_1 [Hz]	**2.13**	**2.32**

Chapter 3: Analytical Model of the Building

To study in more detail the dynamic response of the building, a linear elastic model has been developed using the commercial structural analysis software SAP2000 (Computers and Structures, Inc., 2017). The structural characteristics and material properties of the building have been determined based on available drawings, visual inspection, and data from previous studies. Given that the building is located in the soft-soil area of Mexico City, soil-structure interaction (SSI) has been considered in the model.

3.1: General Modeling Considerations

3.1.1: Materials

Concrete

Concrete elements have a specified compressive strength of f'_c = 24.5 MPa (3350 psi) according to drawings. The modulus of elasticity of concrete has been estimated as $E_c = 3250\sqrt{f'c}$ (MPa) based on the formula proposed by Aire and Murià-Vila (1993). This formula was derived from core data obtained from an existing building in Mexico City with similar characteristics to those of the Durango building. The resulting elastic modulus value, 16090 MPa (~2335 psi), is consistent with recommendations of the Complementary Technical Notes (NTC 2017) of Mexico City for class 1 concrete.

Steel

The steel used in the retrofit is A36 with a modulus of elasticity of 200000 MPa (~29000 ksi). Grade 60 steel is used in the rebar and the same modulus of elasticity has been assumed. No rust or degradation of the steel elements was observed during the visual inspection; therefore, the full stiffness of steel was used in the analysis.

Masonry

Given that no material data is available for the masonry infills. The modulus of elasticity has been taken as $E_m = 2060\ MPa$ ($\sim 300\ ksi$) and the shear modulus as $G_m = 820\ MPa$ ($\sim 120\ ksi$) based on reference values obtained by Arias (2005). These values are representative of a typical clay brick wall built with traditional methods in Mexico.

3.1.2: Geometry

Structural elements have been modeled based on the properties and dimensions obtained from the building drawings, including the floor system and foundation. The model comprises elastic beam and shell elements. Beam elements have been used to model columns, beams, floor joists, foundation ribs, and steel frame braces. Shell elements have been used to model concrete and masonry walls and floor slabs. Details of the building model are shown in Figures 3.1 through 3.5.

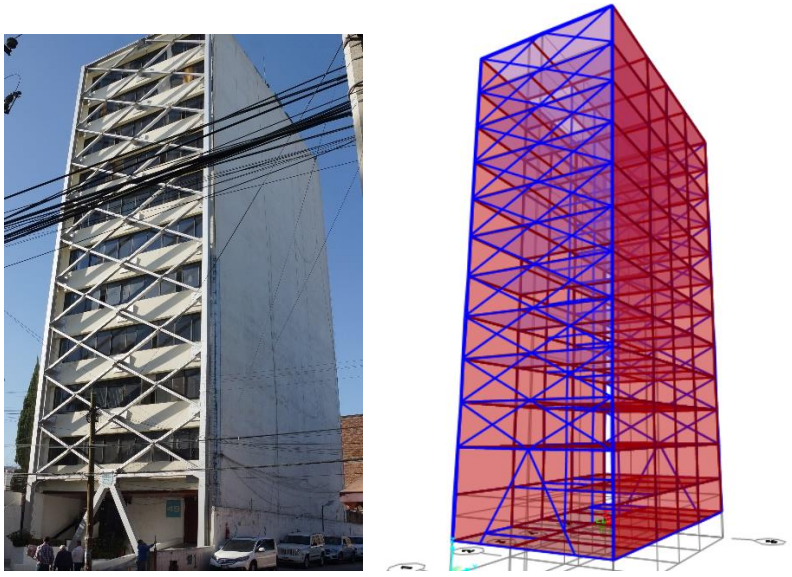

Figure 3.1: Perspectives of the actual building and analytical model

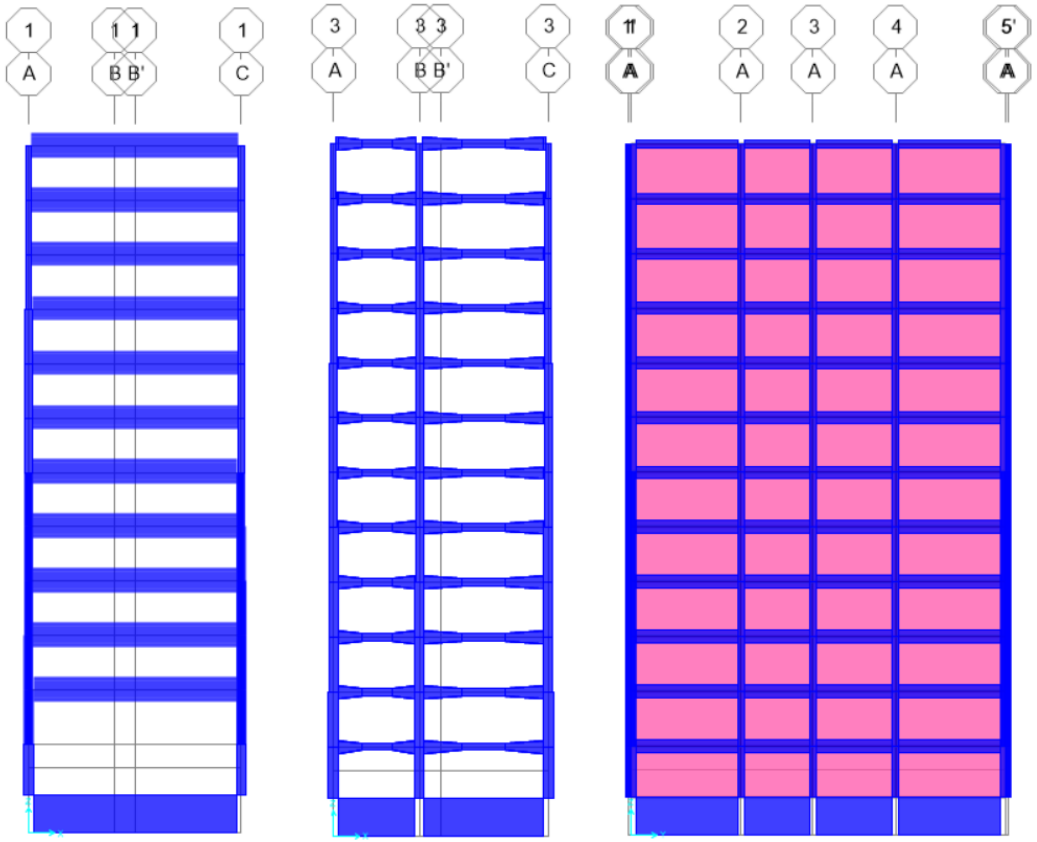

Figure 3.2: Model elevations for Frames 1, 3 and A

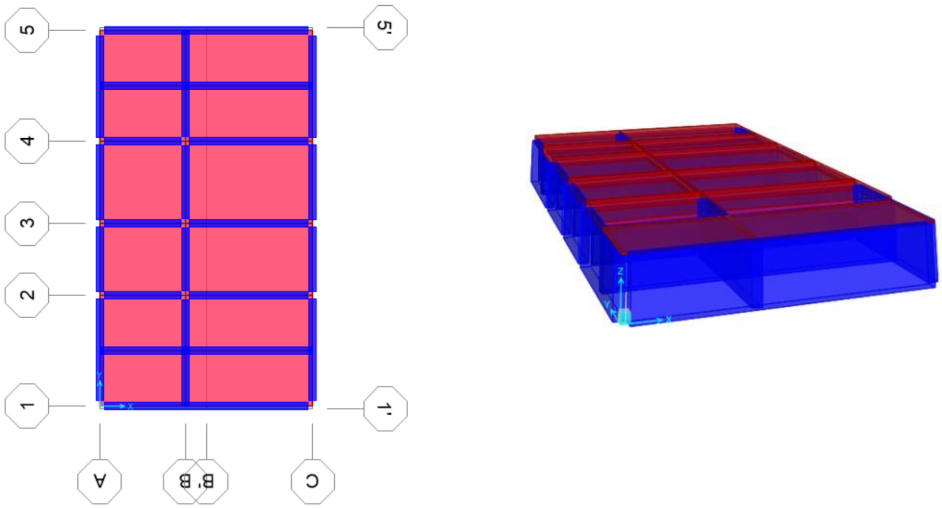

Figure 3.3: Model foundation details

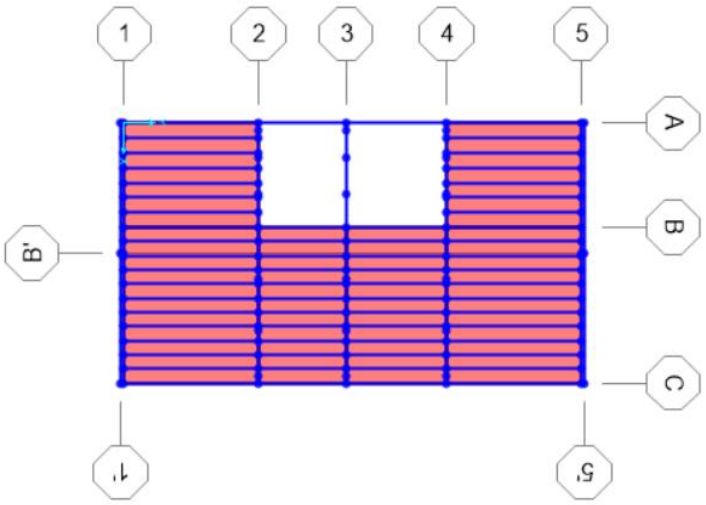

Figure 3.4: Typical floor plan with modeled joists

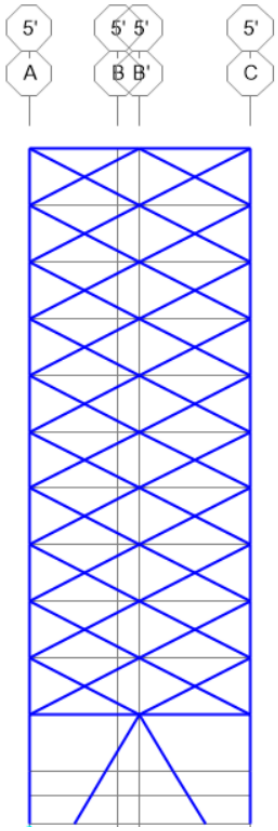

Figure 3.5: Model elevation for steel frame

To facilitate modeling, several simplifications have been introduced. The penthouse has been modeled only as additional mass and load at the top of the roof (Fig. 3.6), and the exterior tapered columns have been modeled using constant average dimensions within a given story as shown in Table 3.1.

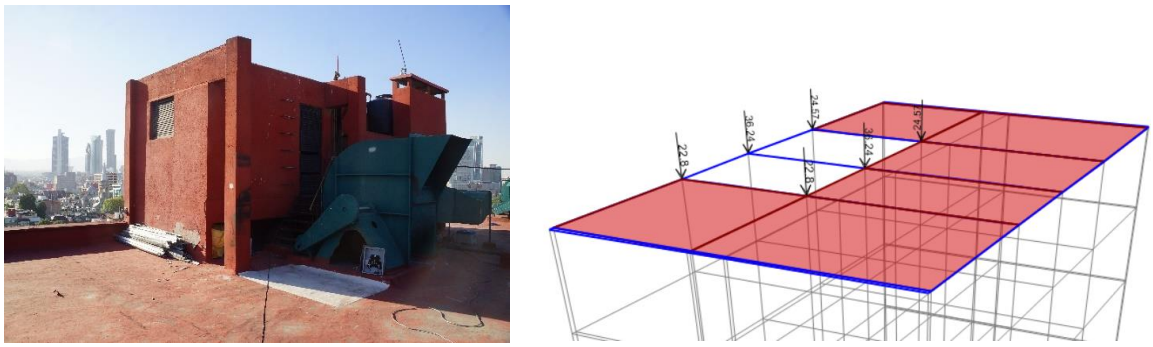

Figure 3.6: Penthouse in building and model

Table 3.1: Column dimensions in model (1 m = 39.37 in)

FLOOR	Type C-1 (b=0.6m) h [m]	Type C-2/3 (b=0.4m) h [m]	Type C-4/5 square column d [m]
ROOF	0.309	0.312	0.35
10	0.328	0.339	0.35
9	0.348	0.365	0.40
8	0.367	0.388	0.40
7	0.387	0.413	0.40
6	0.406	0.438	0.45
5	0.425	0.463	0.45
4	0.444	0.488	0.45
3	0.464	0.514	0.50
2	0.483	0.539	0.50
1	0.502	0.564	0.50
PB	0.521	0.588	0.50
B	0.53	0.6	0.50

The following assumptions have been made regarding the retrofitted elements. Composite sections have been used for the jacketed columns employing the section designer tool for SAP2000 (Fig 3.7). Regarding the concrete infill walls, an equivalent concrete area has been added to the shell elements to account for monolithic action of the 15-cm-thick masonry walls with the concrete walls. The total thickness was computed using the following equation $t = \frac{E_m}{E_c} \cdot t_m + t_c$, for an actual thickness of $t = 0.079m$ ($\sim 3.1\ in$).

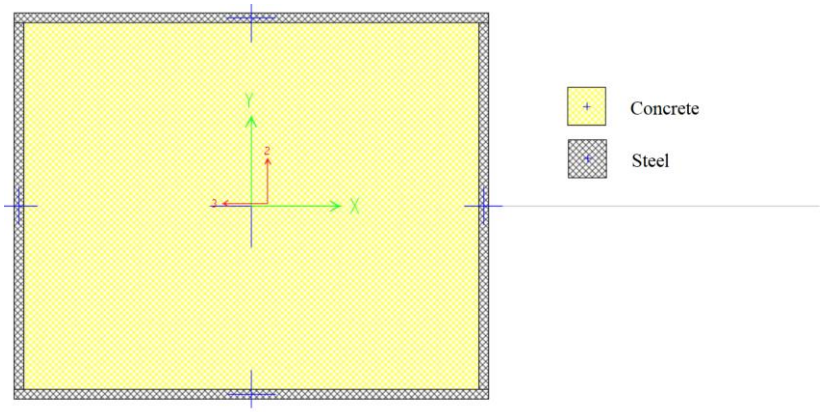

Figure 3.7: Example of composite section

The model has assumed a rigid diaphragm behavior given the in-plane rigidity reported during the forced vibration tests conducted by Downs et al. (1991). This rigid behavior has been represented with a multipoint constraint in the horizontal axis for all nodes in the concrete slab.

3.1.3: Mass, Weight and Gravity Loads

Mass and gravity loads have been based on self-weight of the structure and superimposed loads during normal operation of the building. The latter include non-structural elements and live loads. Superimposed dead and live loads have been uniformly

applied on the floor shell elements. The live load consists of 245 N/m2 (~5.1 psf) for offices, 882 N/m2 (~18.4 psf) for parking spaces, and no live load at the roof level. The additional dead loads are 2403 N/m^2 (~50.2 psf) for offices, 540 N/m^2 (~11.3 psf) for parking spaces and 1080 N/m^2 (~22.6 psf) in the roof. The values obtained have been compared to a previous model developed by Downs et al. (1991) resulting in less than 3% difference in the total mass as shown in Table 3.2. However, the weight distribution in height, which might have an impact on the overall behavior of the building, differs from that of Downs et al. (1991).

Table 3.2: Assumed building weight distribution (1kN=0.225kip)

FLOOR	Current	Downs 1991	Difference
	[kN]	[kN]	%
ROOF+PH	1571	2438	-35.6%
10	2016	1873	7.7%
9	2029	1882	7.8%
8	2087	1935	7.9%
7	2097	1944	7.9%
6	2144	1985	8.0%
5	2170	1995	8.8%
4	2192	2015	8.8%
3	2206	2036	8.3%
2	2220	2046	8.5%
1	2249	2091	7.6%
PB	1760	1673	5.2%
B	6717	6711	60.2%
TOTAL W/O PILES	**31460**	**30623**	2.7%
TOTAL	**35494**	-	-

3.1.4: Effective Stiffness of Elements and Joints

To account for the decrease in stiffness due to flexural cracking of concrete under service loads, the flexural stiffness of the beams has been taken as $0.4E_cI_g$ following ACI 318-14 (2014) recommendations. For calibration purposes, the stiffness of the columns has

been taken as $E_c I_g$ assuming that they were fully compressed during vibration measurements under the action of gravity loads and small amplitude of the ambient vibrations. However, for the time-history analysis ACI recommendation of $0.7E_c I_g$ has been used to account for column decompression during the earthquake motion. Beam-column regions have been represented as rigid zones with the actual dimensions of the joint.

One major difference in the model by Downs et al. (1991) and the one described in this chapter is the reduction of the stiffness in the masonry walls. In the model presented in this thesis, a reduction of 60% in the stiffness of the infill walls was used to account for cracked section assuming that they participate in the lateral load resisting system after being reconnected during the retrofit. This assumption is later verified through a sensitivity study presented in Chapter 4. Downs et al. (1991) on the other hand, assumed that the masonry infills do not participate, using a reduction to their stiffness of 99% to simulate this condition.

3.2: PARTICULAR MODELING CONSIDERATIONS

The Durango building presents some unique characteristics that required further assumptions, including more detailed analysis.

3.2.1: RC-Steel Frame Connection

One important aspect that may affect the behavior of the retrofitted building is the connection between the original structure and the steel frame from the retrofit. The model developed by Downs et. al (1991) assumed that the stiffness of this connection was reduced between 97.5% and 99.8% of its original value to match the fundamental frequency in the E-W direction. This reduction was justified based on the observation of loosened bolts in

some of the anchorage plates in these connections. In the current model, the connection has been considered infinitely stiff to axial and moment forces, and the actual stiffness of the plate elements connecting the steel and concrete frames has been used for shear despite damage reported in a limited number of anchorage plates. This assumption is deemed correct based on the results of the modal analysis and sensitivity studies presented in Chapter 4.

3.2.2: Soil-Structure Interaction (SSI)

Soil-structure interaction (SSI) has been modeled given the soft-soil conditions and the influence of the base displacement and rotation on the overall response of the building as reported from the vibration tests. SSI has been modeled using a single spring with 5 degrees of freedom (DOF), two translational and three rotational. The vertical displacement has been fully restricted. The model assumes the foundation to be a rigid body given the high stiffness of the voided mat. The position of the spring is given by the center of mass of the rigid body with coordinates $x = 5.78\ m$ ($\sim 19\ ft$) and $y = 10.68\ m$ ($\sim 35\ ft$) using as reference the crossing of axis A and 1. The spring constants were computed using Luco's method (Mendoza, et al., 1991). This method requires the following input data: mass distribution (based on Table 3.2), the shape of the 1st mode of a building model with fixed base (see Chapter 4), and experimental dynamic properties of the building (see Chapter 2). Additionally, a modal participation factor (β) and a modal height factor (γ) are computed as shown in the following equations:

$$\beta = \frac{1}{M_1}\{\Phi_1\}^T[M]\{1\} \quad (Eq.\ 3.1)$$

$$\gamma = \frac{1}{HM_1}\{\Phi_1\}^T[M]\{h\} \quad (Eq.\ 3.2)$$

where M_1 and Φ_1 are the modal mass and shape of the first fixed-base natural frequency, M and H correspond to total mass and height, and h the height matrix of the building. With the β and γ parameters and the data previously mentioned we obtain the characteristic frequencies f_H and f_R. These values are directly related to the experimental data obtained through forced or ambient vibration tests and are computed as follows:

$$f_H = \tilde{f}_1 \left(\beta \frac{X_B}{X_T} \right)^{-1/2} \quad (Eq. 3.3)$$

$$f_R = \tilde{f}_1 \left(\gamma \frac{H\theta_B}{X_T} \right)^{-1/2} \quad (Eq. 3.4)$$

Where:

$\tilde{f}_1 = experimental\ fundamental\ frequency$

$X_B = base\ diplacement$

$\theta_B = base\ rotation$

$X_T = roof\ displacement$

Finally, these frequencies are used to determine the horizontal and rotational stiffness coefficients of the foundation by means of the following approximate relations:

$$K_H = \beta^2 M_1 (2\pi f_H)^2 \quad (Eq. 3.5)$$

$$K_R = \gamma^2 M_1 H^2 (2\pi f_R)^2 \quad (Eq. 3.6)$$

Since Luco's method requires the shape of the fixed-base model, the spring coefficients were determined based on the results of the modal analysis presented in Chapter 4. The resulting spring coefficients of the building model are presented in Table 3.3.

Table 3.3: Soil-structure interaction coefficients for final retrofitted model (1 N/m = 0.0685 lb/ft, 1 N-m = 0.737 lb-ft)

DIRECTION	COEFFICIENT	
Transverse Traslation	7.084E+08	N/m
Transverse Rotation	7.131E+10	N-m/rad
Longitudinal Translation	9.626E+08	N/m
Longitudinal Rotation	1.232E+11	N-m/rad
Torsional Rotation	1.814E+11	N-m/rad

Chapter 4: Modal Analysis and Sensitivity Study

4.1: MODAL ANALYSIS

The results of the ambient vibration test from 2017 were used to calibrate the SSI and to validate the model presented in Chapter 3. This process required two models: one with a fixed base and another one with SSI. A modal analysis was performed for both models to determine the analytical vibration frequencies and modes and compare them to the dynamic properties obtained experimentally.

4.1.1: Fixed Based Model

The vibration frequencies and modes of the structure considering a fixed base are presented in Table 4.1 alongside a comparison with the model proposed by Downs et al (1991). There we can notice the higher N-S and rotational frequencies (2.31 Hz and 2.49 Hz respectively) of the building when compared to the E-W direction (1.18 Hz). This is consistent with the much higher stiffness of the RC frames and infill walls in the east and west façades when compared to the combination of the steel and RC frames. The three fundamental modes are illustrated in Figures 4.1 through 4.3.

Additionally, the dynamic properties of the fixed base model obtained here and that proposed by Downs et al. (1991) highly differ in the directions where the infill walls are involved (N-S and torsional). This is due to a core difference between the models, which is the reduction to only 1% of the actual masonry stiffness in the model by Downs et al. (1991) as compared to the 60% reduction in the fixed base model presented here, as explained in Section 3.1.4. Higher participation of the masonry walls in the response of the building is assumed here considering that these walls are not isolated from the frame. This assumption is consistent with cracks observed in some masonry walls after the 2017 earthquake (Fig. 4.4) and the data from the 2017 AVT. The participation of the masonry

walls also affects the torsional modes given the external position in the plan of the building. This is further discussed based on a sensitivity study presented in Section 4.2.3. On the other hand, the fundamental frequency in the E-W is very similar for both models despite the difference in the RC-steel frame connection assumptions. This is probably related to differences in the stiffness provided to the rest of the structural elements.

Table 4.1: Fixed base model comparison

Direction		Fixed Base	Downs 1991	Difference
E-W (T)	f_1 [Hz]	**1.18**	**1.12**	**5%**
	f_2 [Hz]	3.42	2.79	23%
	f_2/f_1	2.89	2.48	17%
N-S (L)	f_1 [Hz]	**2.31**	**1.59**	**45%**
	f_2 [Hz]	7.08	4.02	76%
	f_2/f_1	3.07	2.52	22%
Torsional	f_1 [Hz]	**2.49**	**1.87**	**33%**
	f_2 [Hz]	7.31	-	-
	f_2/f_1	2.94	-	-

4.1.2: Model with Soil-Structure Interaction

The model with SSI was developed using a single spring located at the base of the building as described in Chapter 3. The modal shapes of the model with SSI are illustrated in Figures 4.1 through 4.3 and the dynamic properties presented in Table 4.2. These results show the level of accuracy achieved, with all three fundamental modes (E-W, N-S, torsion) within 5% of the vibration frequencies obtained from the ambient vibration tests. Additionally, the ratios between the first and second modes, 3.48 in the E-W direction and 3.09 in the N-S direction, indicate that the overall behavior of the building is closer to that of a shear cantilever than a flexural cantilever. While these values are smaller than those obtained in the AVT, the addition of the soil spring contributes to increase the ratios and

move this behavior closer to that of a flexural beam, as depicted from the comparison of Tables 4.1 and 4.2.

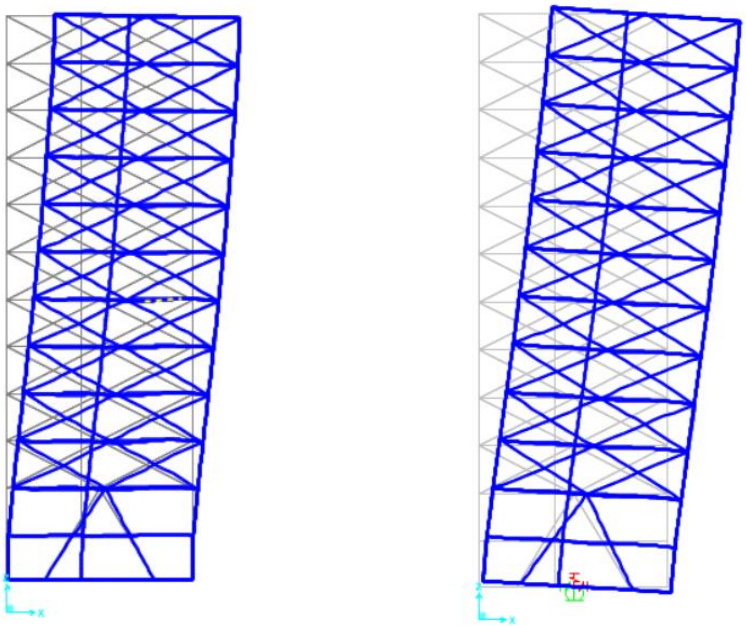

Figure 4.1: Mode 1 in E-W direction with fixed base (1.18 Hz) and SSI (0.81 Hz)

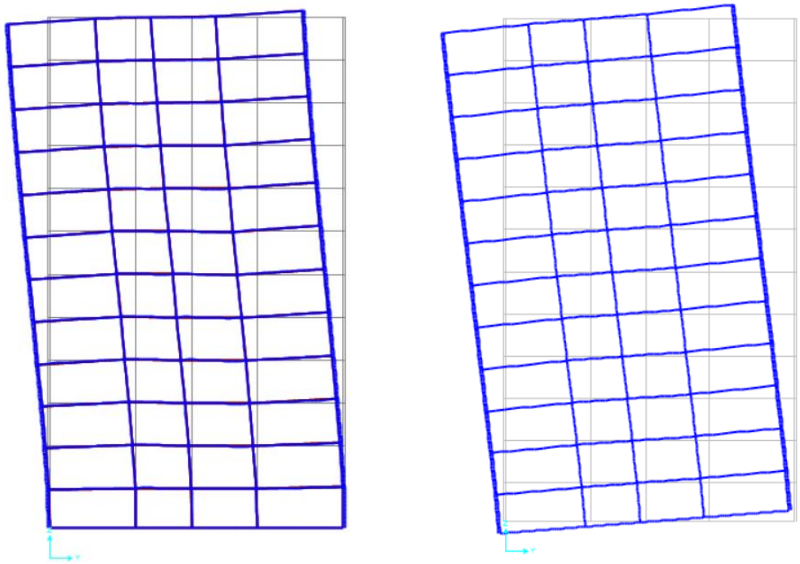

Figure 4.2: Mode 1 in N-S direction with fixed base (2.31 Hz) and SSI (1.19 Hz)

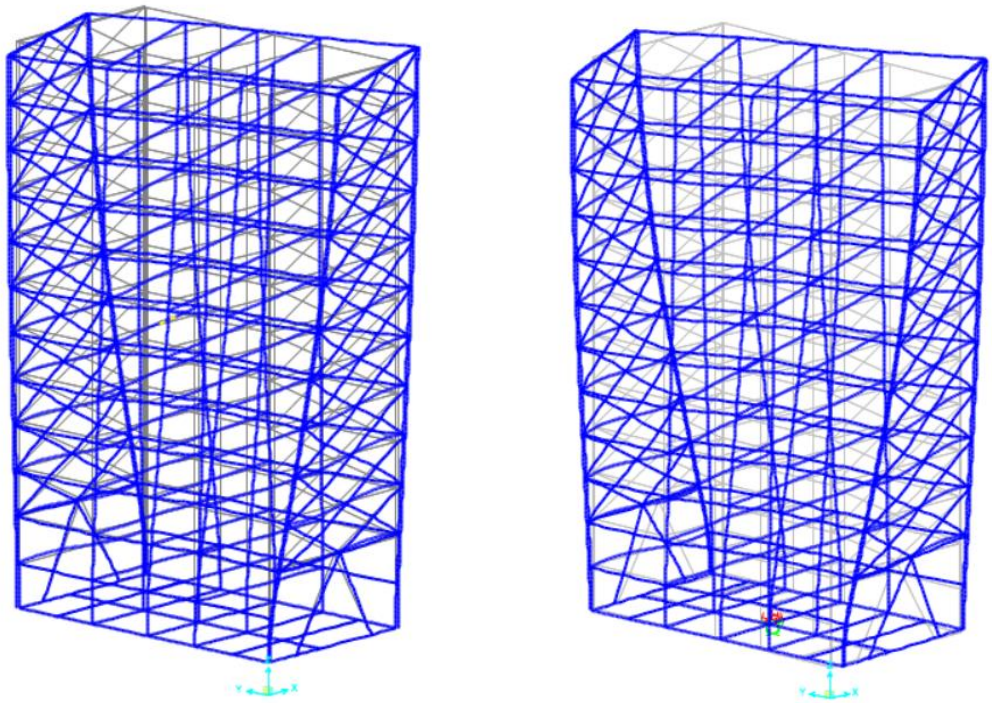

Figure 4.3: First torsional mode with fixed base (2.49 Hz) and SSI (2.25 Hz)

Figure 4.4: Damage to masonry wall from September 19th, 2017 earthquake

Table 4.2: Analytical and experimental vibration frequencies (model with SSI vs. AVT 2017)

Table 4.2: SSI Model Vs. AVT 2017				
Direction		SSI	AVT 2017	Difference
E-W (T)	f1 [Hz]	**0.81**	**0.85**	**-5%**
	f2 [Hz]	2.82	3.59	-21%
	f2/f1	3.48	4.20	-17%
N-S (L)	f1 [Hz]	**1.19**	**1.25**	**-4%**
	f2 [Hz]	3.70	5.27	-30%
	f2/f1	3.09	4.23	-27%
Torsional	f1 [Hz]	**2.25**	**2.32**	**-3%**
	f2 [Hz]	5.99	-	-
	f2/f1	2.66	-	-

The results of the modal analysis highlight the importance of the SSI for this building. The addition of foundation flexibility (Table 4.3) increases 46% the fundamental period in the E-W direction and 93% in the N-S direction. Another important piece of information obtained from the analysis is the participation of translation and rotation at the base to the roof displacements (Table 4.4). As shown, the base flexibility accounts for 52.8% and 72.8% of the roof displacement in the E-W and N-S direction, respectively. While the values are not exactly the same, these results are consistent with the conclusions of the AVT performed 2017 which also showed over that 50% of the roof translation was caused by base flexibility (see Table 4.4).

Table 4.3: Vibration frequencies for fixed base model vs. SSI Model

Direction		Fixed Base	SSI	Difference
E-W (T)	f_1 [Hz]	**1.18**	**0.81**	**46%**
	f_2 [Hz]	3.42	2.82	21%
	f_2/f_1	2.89	3.48	-17%
N-S (L)	f_1 [Hz]	**2.31**	**1.19**	**93%**
	f_2 [Hz]	7.08	3.70	92%
	f_2/f_1	3.07	3.09	-1%
Torsional	f_1 [Hz]	**2.49**	**2.25**	**11%**
	f_2 [Hz]	7.31	5.99	22%
	f_2/f_1	2.94	2.66	10%

Table 4.4: Base motion participation in roof displacement

Direction	Motion	SSI Model	AVT 2017
		% of Roof Disp.	% of Roof Disp.
E-W (T)	Trans.	5.5%	5.7%
	Rotation	47.3%	57.6%
	Total	**52.8%**	**63.3%**
N-S (L)	Trans.	9.0%	7.3%
	Rotation	63.8%	59.0%
	Total	**72.8%**	**66.3%**
Torsional	Rotation	**14.5%**	**12.7%**

4.2: SENSITIVITY ANALYSIS

A parametric study was conducted using modal analysis to measure the impact of several variables and assumptions in the dynamic properties of the Durango building. This analysis was done to support the calibration of the model and verify some of the adopted assumptions. The following section presents the different variables used in the sensitivity analysis and their overall influence in the analytical results.

4.2.1: Weight

Given the variable and approximate nature of the superimposed loads, variations in these loads were considered in this sensitivity study. There was a high degree of confidence

in the initial assumptions, so these loads were only modified to have an additional perspective of the effects. Two additional models were created one with an increase of 20% to the superimposed dead and live loads (self-weight is excluded) described in Section 3.1.3, and the other with a reduction of the same magnitude. The total change in weight is presented in Table 4.5, which shows how a 20% change in superimposed loads is reduced to less than 6% when the structure self-weight is added.

The natural frequencies of the building with a fixed base change by less than 5% (Table 4.6), showing a proportional increase/reduction of the frequencies for E-W, N-S, and torsional modes. It is also important to note that the ratios between the first and second modes remain the same.

Adding the effects of the soil-structure interaction (Table 4.7) the effects of the change in mass are reduced even further. From ~4% to less than 2%, with the exception being the translational mode. This can be attributed to the change in the spring values of around 8% (Table 4.8), given that mass is a factor used in Luco's method, and the high participation of the base displacements and rotations mentioned in earlier in this chapter.

Table 4.5: Weight comparison for calibration (1 kN = 0.225 kip)

FLOOR	Base Model	20% Increase Model		20% Reduction Model	
	Weight	Weight	Difference	Weight	Difference
	[kN]	[kN]	%	[kN]	%
PH+R	1571	1654	5.3%	1454	-7.4%
10	2016	2194	8.8%	1839	-8.8%
9	2029	2206	8.8%	1851	-8.8%
8	2087	2265	8.5%	1910	-8.5%
7	2097	2274	8.5%	1919	-8.5%
6	2144	2322	8.3%	1966	-8.3%
5	2170	2348	8.2%	1993	-8.2%
4	2192	2370	8.1%	2015	-8.1%
3	2206	2384	8.0%	2029	-8.0%
2	2220	2397	8.0%	2042	-8.0%
1	2249	2427	7.9%	2072	-7.9%
PB	1760	1866	6.0%	1654	-6.0%
B	6717	6717	0.0%	6717	0.0%
PILES	4035	4035	0.0%	4035	0.0%
TOTAL W/O PILES	**31460**	**33424**	**6.2%**	**29461**	**-6.4%**
TOTAL	**35494**	**37459**	**5.5%**	**33496**	**-5.6%**

Table 4.6: Fixed base dynamic properties calibration comparison (weight)

		Base	20% Increase	20% Reduction
E-W (T)	f1 [Hz]	1.18	1.14	1.24
	Diff.	-	***-3.8%***	***4.4%***
	f2 [Hz]	3.42	3.30	3.57
	Diff.	-	***-3.7%***	***4.3%***
	f2/f1	2.89	2.90	2.89
N-S (L)	f1 [Hz]	2.31	2.22	2.41
	Diff.	-	***-3.8%***	***4.4%***
	f2 [Hz]	7.08	6.83	7.37
	Diff.	-	***-3.6%***	***4.1%***
	f2/f1	3.07	3.07	3.06
Torsional	f1 [Hz]	2.49	2.40	2.59
	Diff.	-	***-3.6%***	***4.1%***
	f2 [Hz]	7.31	7.05	7.60
	Diff.	-	**-3.5%**	**4.0%**
	f2/f1	2.94	2.94	2.93

Table 4.7: SSI dynamic properties calibration comparison (weight)

		Base w/SSI	20% Increase w/SSI	20% Reduction w/SSI
E-W (T)	f1 [Hz]	0.81	0.80	0.83
	Diff.	-	***-1.8%***	**1.9%**
	f2 [Hz]	2.82	2.80	2.84
	Diff.	-	***-1.0%***	**0.6%**
	f2/f1	3.48	3.51	3.44
N-S (L)	f1 [Hz]	1.19	1.18	1.21
	Diff.	-	***-0.9%***	**0.9%**
	f2 [Hz]	3.70	3.75	3.62
	Diff.	-	***1.6%***	**-2.0%**
	f2/f1	3.09	3.17	3.00
Torsional	f1 [Hz]	2.25	2.18	2.32
	Diff.	-	***-2.9%***	**3.1%**
	f2 [Hz]	5.99	5.93	6.04
	Diff.	-	**-0.9%**	**0.8%**
	f2/f1	2.66	2.72	2.60

Table 4.8: Base motion participation in roof displacement and new spring coefficients (1 N/m = 0.0685 lb/ft, 1 N-m = 0.737 kip-ft)

			Base w/SSI	20% Increase w/SSI	20% Reduction w/SSI
Contribution of SSI to Roof Displacement	E-W (T)	Trasl.	5.5%	5.3%	5.8%
		Rot.	47.3%	46.7%	49.9%
	N-S (L)	Trasl.	9.0%	8.8%	9.2%
		Rot.	63.8%	62.4%	64.8%
	Torsional		14.5%	13.4%	15.8%
Spring Constant (N/m, N-m/rad)	E-W (T)	Trasl.	7.08E+08	7.66E+08	6.50E+08
		Rot.	7.13E+10	7.70E+10	6.54E+10
	N-S (L)	Trasl.	9.63E+08	1.04E+09	8.82E+08
		Rot.	1.23E+11	1.33E+11	1.13E+11
	Torsional		1.81E+11	1.95E+11	1.67E+11

4.2.2: Concrete Stiffness

To measure the effects of the concrete modulus of elasticity, two additional models were considered. In one model the concrete stiffness was reduced to what the Mexico

City's Complementary Technical Notes (NTC 2017) considers class 2 concrete ($Ec = 12375\ MPa$ this case), or an equivalent reduction of 23%. The second model was modified with an increase of 25% to 20112.5 MPa.

The modal analyses results showed that the changes in dynamic properties (Table 4.9) was concentrated in the N-S and torsional directions (±5% and ±4% respectively), while the E-W mode varies around 2.5%. The small variation in the E-W direction can be explained by the high stiffness of the steel frame which governs the response. This concurs with the design assumptions of the retrofit. Additionally, it can be noticed that the ratios between 2nd and 1st mode remain almost the same, with only slight increases/reductions proportional to the stiffness of the concrete. This can be interpreted as the stiffness of the concrete not having a relevant impact on the overall behavior of the building.

Table 4.9: Fixed base dynamic properties calibration comparison (concrete stiffness)

		Base	Class 2 Conc.	25% Higher Ec
E-W (T)	f1 [Hz]	1.18	1.15	1.21
	Diff.	-	***-2.6%***	***2.6%***
	f2 [Hz]	3.42	3.34	3.51
	Diff.	-	***-2.5%***	***2.6%***
	f2/f1	2.89	2.90	2.89
N-S (L)	f1 [Hz]	2.31	2.19	2.43
	Diff.	-	***-5.3%***	***5.1%***
	f2 [Hz]	7.08	6.64	7.51
	Diff.	-	***-6.2%***	***6.0%***
	f2/f1	3.07	3.04	3.10
Torsional	f1 [Hz]	2.49	2.40	2.58
	Diff.	-	***-3.4%***	***3.5%***
	f2 [Hz]	7.31	7.03	7.61
	Diff.	-	**-3.8%**	**4.1%**
	f2/f1	2.94	2.92	2.95

4.2.3: Masonry Infill

The models presented in this section were intended to determine if the masonry infills were contributing or not to the stiffness of the building in the N-S direction. One model considers a reduced stiffness of the masonry to the levels recommended by the Complementary Technical Notes (NTC 2017) when no testing is provided ($Em = 1200\ MPa$), equivalent to a 42% reduction in stiffness. The second model eliminates altogether the masonry infills in bays 2-3 and 3-4 of Frames A and C as shown in Fig. 4.5.

The results in Table 4.10 show a difference in the dynamic properties in the longitudinal (N-S) and torsional directions when compared to the reference fixed-base model. The model with lower masonry stiffness presents a reduction of 10.3% and 6.3% for the N-S and torsional fundamental modes respectively. On the other hand, the model with no masonry infills presents a larger reduction of 39% in N-S direction and 19.5% in the torsional direction.

These important differences in fundamental frequencies and the damage observed in some masonry walls mentioned earlier in this chapter confirm the assumption that the masonry walls participate in the overall building response.

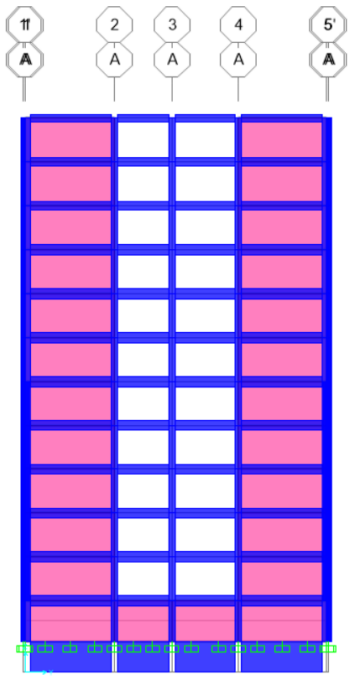

Figure 4.5: N-S Elevation of axis A without masonry infill (white)

Table 4.10: Fixed base dynamic properties calibration comparison (masonry infill)

		Base	CTN (2017)	No Infill
E-W (T)	f1 [Hz]	1.18	1.18	1.18
	Diff.	-	***-0.3%***	***-0.3%***
	f2 [Hz]	3.42	3.41	3.42
	Diff.	-	***-0.3%***	***-0.3%***
	f2/f1	2.89	2.89	2.90
N-S (L)	f1 [Hz]	2.31	2.07	1.41
	Diff.	-	***-10.3%***	***-39.0%***
	f2 [Hz]	7.08	6.51	5.28
	Diff.	-	***-8.1%***	***-25.5%***
	f2/f1	3.07	3.14	3.74
Torsional	f1 [Hz]	2.49	2.33	2.00
	Diff.	-	***-6.4%***	***-19.5%***
	f2 [Hz]	7.31	6.83	5.90
	Diff.	-	**-6.5%**	**-19.2%**
	f2/f1	2.94	2.93	2.95

4.2.4: Joint Stiffness

A limited sensitivity study was conducted on the joint stiffness. To this end, an additional model was built reducing the stiffness of the joint by 50%. This reduction increases the effective length of the column while being computed by the software.

The results in Table 4.11 show changes to the natural frequencies below 2% in the transverse direction (E-W) and less than 1% in the longitudinal (N-S) and torsional modes.

Table 4.11: Fixed base dynamic properties calibration comparison (joint stiffness)

		Base	Joint 50%
E-W (T)	f1 [Hz]	1.18	1.17
	Diff.	-	***-1.1%***
	f2 [Hz]	3.42	3.37
	Diff.	-	***-1.7%***
	f2/f1	2.89	2.88
N-S (L)	f1 [Hz]	2.31	2.30
	Diff.	-	***-0.5%***
	f2 [Hz]	7.08	7.03
	Diff.	-	***-0.7%***
	f2/f1	3.07	3.06
Torsional	f1 [Hz]	2.49	2.47
	Diff.	-	***-0.7%***
	f2 [Hz]	7.31	7.25
	Diff.	-	**-0.8%**
	f2/f1	2.94	2.93

The small reduction confirms that the joint stiffness assumption does not significantly affect the response of the building, which is due to the fact that the steel frame is resisting most of the lateral load as Del Valle intended (Downs, et al., 1991). In the other direction, the infill walls also limit the effect of the joint stiffness assumption.

4.2.5: Stiffness of RC-Steel Frame Connections

Possible variations in the response of the building due to damage in the connection between the original structure and the steel frame added during the retrofit were studied by

modifying the stiffness of the connecting elements. This analysis is relevant especially after the damage during the 2012 earthquake that loosened some connections. A model with this connection's shear stiffness reduced by 99% was subjected to modal analysis and the results compared to the base model. The results in Table 4.12 show that the response of the building in the direction of interest for this analysis (E-W) changes in 7.7% for the 1st mode and 12.3% in the 2nd. Also, the change in the connection has an effect on the torsional modes (7.5% for the 1st mode and 5% for the second).

Additionally, the ratio between the 2nd and 1st mode in the E-W direction presents a reduction of 5% in the model with reduced connection stiffness. This indicates that the behavior of the structure gets closer to a shear cantilever. Since this is the opposite of what is needed to better approach the experimental data, the assumption that there is no reduction in the connection stiffness is considered correct.

Table 4.12: Fixed base dynamic properties calibration comparison (RC-steel conn.)

		Base	Reduced Conn. 99%
E-W (T)	f1 [Hz]	1.18	1.09
	Diff.	-	***-7.7%***
	f2 [Hz]	3.42	3.00
	Diff.	-	***-12.3%***
	f2/f1	2.89	2.75
N-S (L)	f1 [Hz]	2.31	2.26
	Diff.	-	***-2.3%***
	f2 [Hz]	7.08	6.62
	Diff.	-	***-6.5%***
	f2/f1	3.07	2.93
Torsional	f1 [Hz]	2.49	2.30
	Diff.	-	***-7.5%***
	f2 [Hz]	7.31	6.94
	Diff.	-	**-5.0%**
	f2/f1	2.94	3.01

4.2.6: Final Remarks on the Sensitivity Analysis

The sensitivity analysis was very useful to calibrate the model and support the assumptions made to represent the behavior of the Durango building.

The soil-structure interaction proved to be a major factor in the building deformation having over 50% of the participation in the roof displacement. The inclusion of the masonry infill walls in the model was adequate since the stiffness provided increases the natural frequencies of the N-S and torsional modes to levels closer to the experimental data. Concrete stiffness provided some additional adjustment to calibrate the building behavior given the effects it has on the longitudinal (N-S) and torsional response. There was no reduction of stiffness to the connection between the RC frame and the steel frame added after the retrofit, given the negative effect it had in the ratio of the 1st and 2nd frequency modes in the E-W direction.

On the other hand, joint stiffness appeared to have minimum participation in the overall behavior of the building. The effects of superimposed loads, while contributing to the weight of the building and later the SSI, on the dynamic properties proved to be minor.

The final model containing the refinement of the variables mentioned in this in this chapter presented predicted dynamic properties within 5% of the data from the most recent ambient vibration test provided by Dr. Murià-Vila, making it a good approximation that can be used for linear elastic analysis.

Chapter 5: Time-History Dynamic Analysis

After the calibration of the Durango building model, linear elastic time-history dynamic analyses were conducted to assess the response of the building during the 1985 and 2017 earthquakes in Mexico City. This chapter includes a description of the time-history dynamic analyses, including the selection of ground motions, and computed response of the building to the 1985 and 2017 motions.

5.1: EARTHQUAKE MOTION RECORDS

5.1.1: Motion Record Selection

Since there are no ground motion records at the exact building location, accelerograms from nearby sites were used. To select these records, the unique characteristics of Mexico City's soil require special attention given that the depth of soft soil has a very important effect on the intensity of the shaking.

The current building code in Mexico City (NTC 2017) divides the city into 3 zones: hill zone (rock), transition zone and lake zone (soft soil) (I to III), to account for this effect. In previous code versions (NTC 2004) the lake zone was later subdivided into 4 zones according to soft soil depth (IIIa to IIId), with our building localized in zone IIIb. Even though this subdivision is no longer used for new designs, the principles are still valid and zone IIIb was used as a condition when selecting the motion records considering similar soil conditions.

Two stations were selected following the conditions above, CO56 and SCT. As shown in figure 5.1, CO56 was selected due to its proximity to the building (only 180m away) while SCT was selected given the availability of records for the two earthquakes to be analyzed given that CO56 was installed only after 1985. A summary of the characteristics of the motions recorded by these stations is presented in Table 5.1.

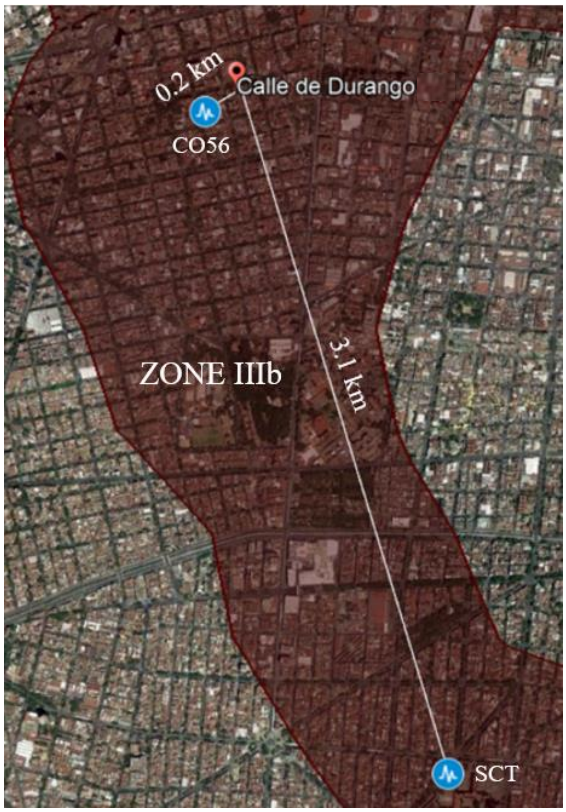

Figure 5.1: Motion record localization relative to building.

Table 5.1: Ground motion record summary

	1979 SCT	1985 SCT	2017 SCT	2017 CO56
Duration of Record [sec]	45	185	300	350
Duration of Strong Shaking* [sec]	15	55	55	65
Peak Ground Acceleration [g]				
N-S	0.034	0.10	0.093	0.11
E-W	0.031	0.17	0.094	0.12
5% Peak Spectral Acceleration [g]				
N-S	0.17	0.63	0.38	0.46
E-W	0.12	0.96	0.60	0.33

*strong shaking is considered accelerations of magnitude higher than 0.03 g

5.1.2: September 19th, 2017 Earthquake

For the most recent earthquake, the record from station CO56 (Figure 5.2) was considered the most appropriate given the distance to the building site, but to keep consistency with the other events, SCT station is also included in the analysis. Additionally, having two records of the same event can illustrate how the local conditions affect the analysis and the record itself.

Even though CO56 and SCT records are from the same event and have similar soil conditions, they present some differences. The duration of strong shaking (~65 and ~55 seconds respectively) and the N-S to E-W peak acceleration proportion are very similar, but the CO56 motion has 30% higher peak acceleration in both directions with 0.11g and 0.12g in the N-S and E-W direction respectively. This difference confirms the important effect of the local soil conditions in the analysis even when both stations are localized in the same seismic zone.

Further differences can be seen in the response spectra from Figure 5.3 with their shape only matching in certain period ranges. In the E-W direction between 0s and 0.5s, at 1.35s and 1.9s. In the N-S direction, their shape is similar up to 0.6s, the range between 1 and 1.4s and at 2s. Additionally, the spectral accelerations specific for the building fundamental periods (Table 5.2) show and reduction of 4% in the translational (EW) direction and 54% in the longitudinal (NS) direction when comparing the SCT record to CO56.

The inconsistencies between the two records should be considered when interpreting the response of the building. All the results obtained by the SCT station will be used for qualitative comparison with the more accurate data obtained using the record at the CO56 station, given the later closer proximity to the site of interest.

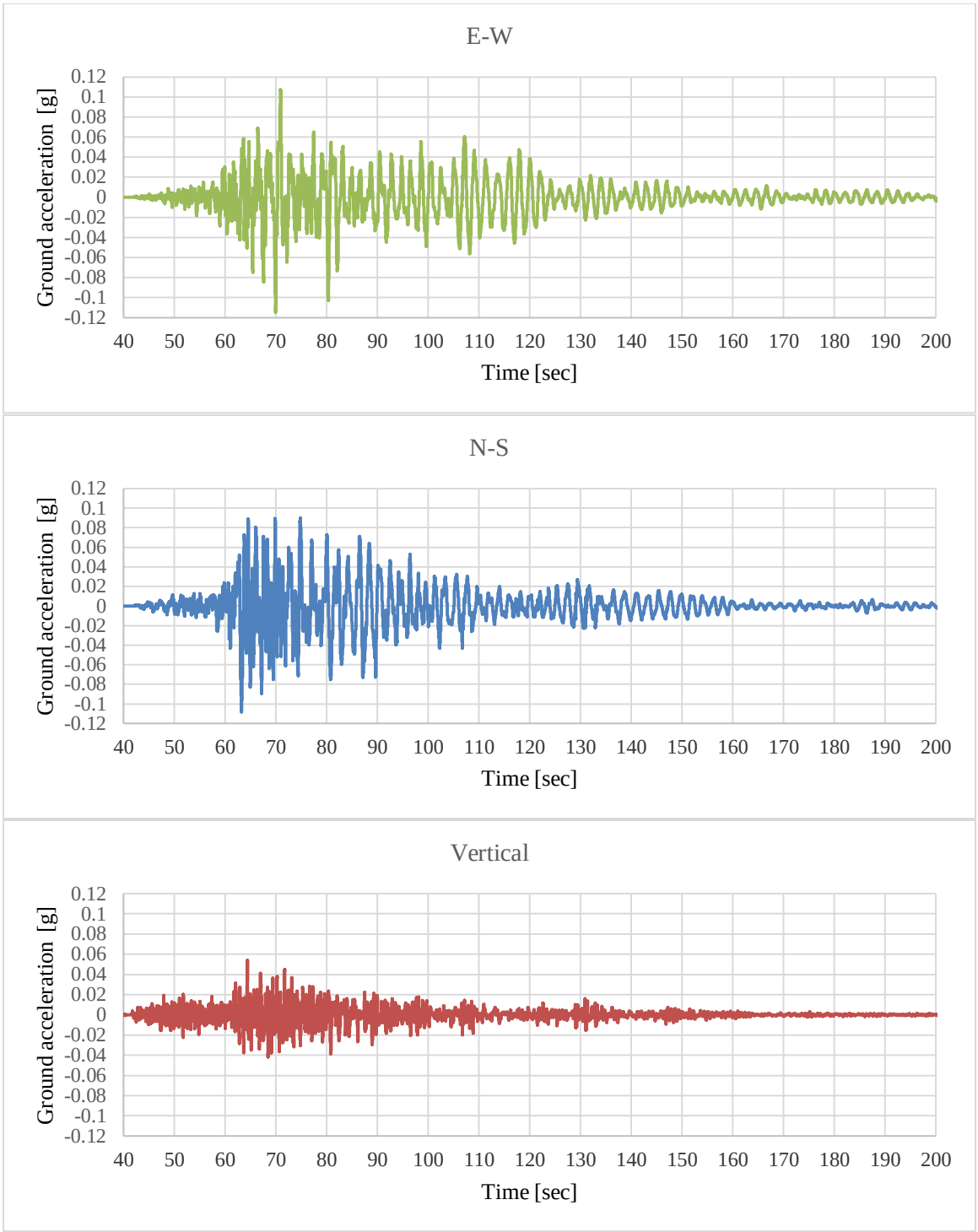

Figure 5.2: CO56 motion record for September 19th, 2017 earthquake

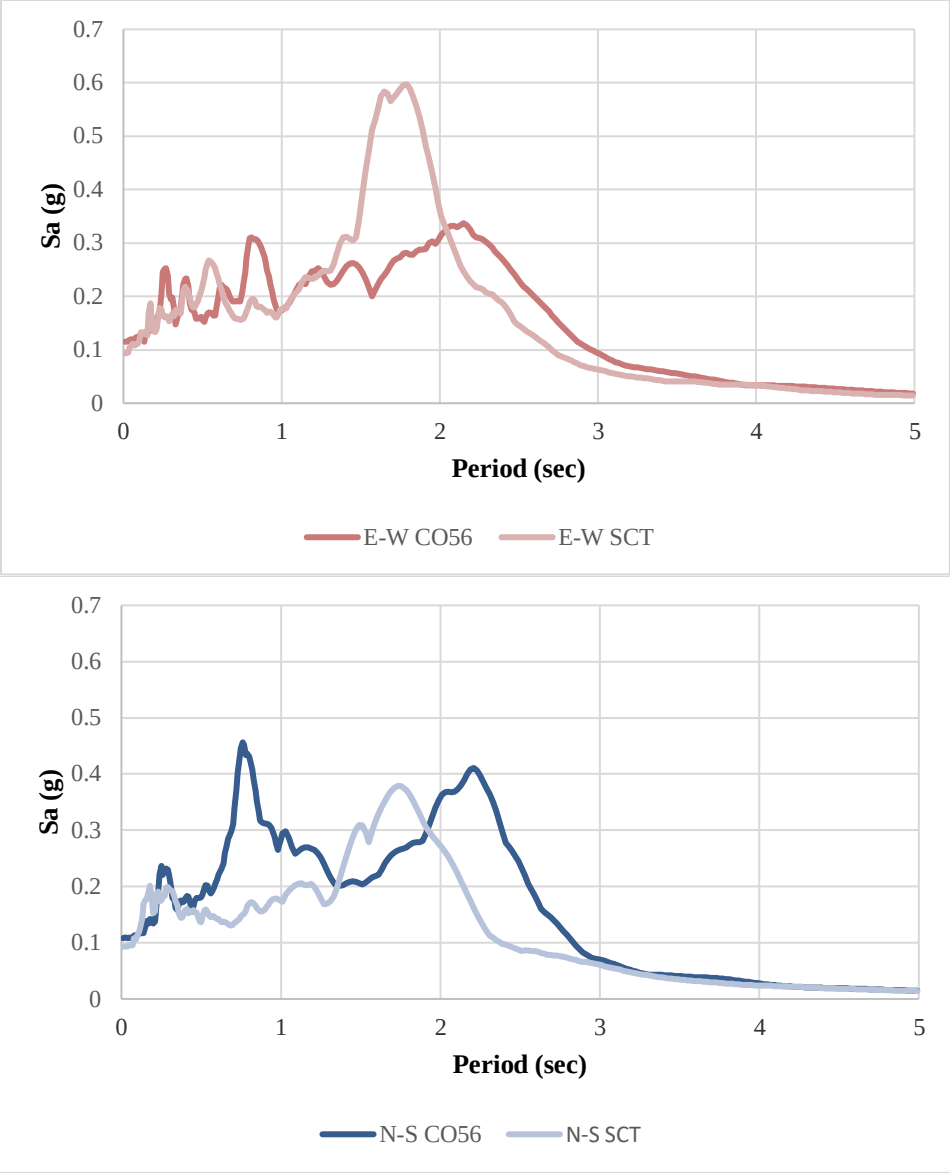

Figure 5.3: 2017 SCT and CO56 5% Response spectra comparison

Table 5.2: Spectral acceleration for building fundamental periods (model with SSI) in 2017 earthquake

	E-W	N-S
Fundamental Period [sec]	1.23	0.84
CO56 2017 Sa [g]	**0.25**	**0.37**
SCT 2017 Sa [g]	**0.24**	**0.17**
Difference	-4%	-54%

5.1.3: September 19th, 1985 Earthquake

For the 1985 earthquake, only the SCT station record was available. Contrary to the 2017 record, a major difference in peak accelerations is present between N-S and E-W direction with the latter being higher by a ~70% (0.10g vs. 0.17g). This difference is also presented in the response spectra shown in Figure 5.4, where the higher accelerations are concentrated around T=2 sec with a maximum spectral acceleration of 0.96 g.

However, at the point of the natural frequencies of our building the spectral accelerations are much lower with values of 0.26 g and 0.17 g for the E-W and N-S direction respectively. As shown, the spectral acceleration in the longitudinal direction of the building is significantly smaller than the 0.37g of the 2017 CO56 record. However, these values should be analyzed with caution given the distance from the SCT station to the actual building site and possible differences in local soil conditions.

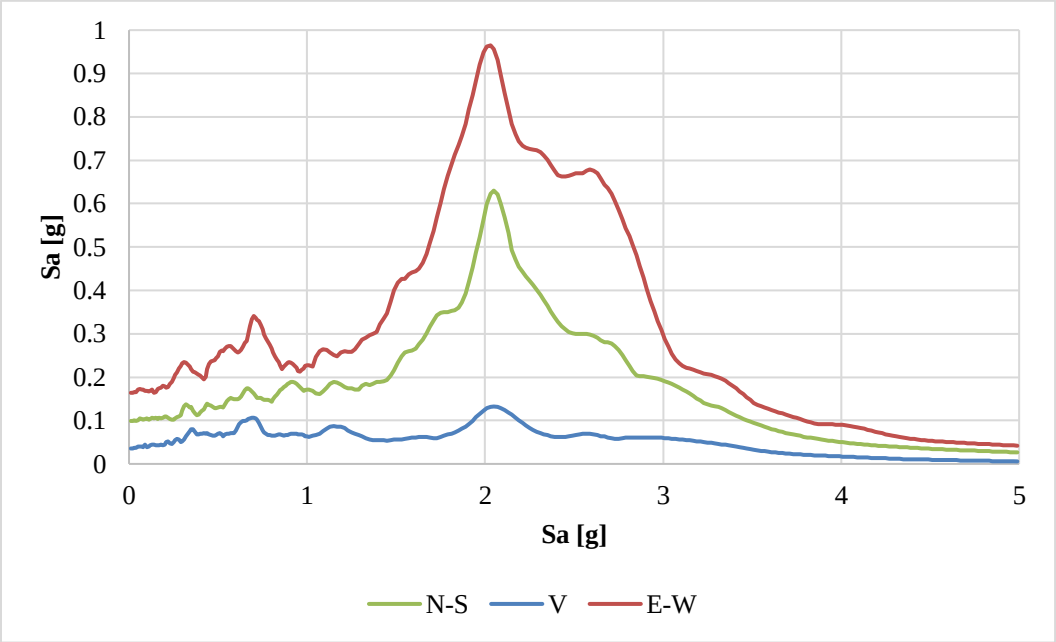

Figure 5.4: 1985 SCT 5% Response spectra

5.2: LINEAR ELASTIC TIME-HISTORY ANALYSIS

To better understand the behavior of the building and the effectiveness of the retrofit several linear elastic time-history analyses have been conducted. The linear elastic assumption has been considered appropriate given the absence of structural damage observed during the 1985 and 2017 events. The linear elastic assumption has been verified based on the force demands obtained from the analyses, specifically the structural elements that presented damage in the 1979 earthquake prior to the retrofit.

The horizontal motions were introduced to the model with an angle of 12 degrees to the east given that the axes of the building are not perfectly aligned with the N-S and E-W directions. Additionally, a damping ratio of 5% was used in the analysis as is typically implicit in codes (Chopra, 2012), which remains constant throughout all the vibration modes.

Four different analyses were conducted. The first one corresponds to the building model with SSI subjected to the 2017 CO56 motion. A second analysis was conducted with this same motion using the fixed base model to determine the effects of SSI. The third analysis was conducted with the building model with SSI subjected to the 2017 SCT motion to understand the effects of local soil conditions. Finally, an analysis of the building model with SSI subjected to the 1985 SCT motion was conducted to analyze the response of the building to this event.

5.2.1: TH Analysis: Station CO56 Ground Motion Record from September 19th, 2017

The first analysis used the CO56 ground motion record to have the closest approximation to the actual behavior of the building given its proximity to the site. This analysis will be later used as a base for comparison with the other analyses.

The main characteristics of the response of the Durango building to the 2017 CO56 motion are summarized in Table 5.3. The first parameter evaluated is the maximum base shear, which presents values of 0.23*W* in the E-W direction and 0.30*W* in the N-S direction, where *W* is the weight of the building. These values show the importance of the retrofit given the original shear capacity determined by Downs et al. (1991) of 0.14*W*. The additional stiffness provided by the retrofit also highly reduces the roof displacements, keeping them well below the Mexico City's current Complimentary Technical Notes (NTC 2017) limit of 0.006*H,* with 0.0037*H* and 0.0023*H* for the transverse and longitudinal direction, respectively. Additionally, Figures 5.5 through 5.8 show the change in base shear and roof drift over time.

Table 5.3: Time-history CO56 base shear and roof displacement (1 kN = 0.225 kip, 1 m = 39.37in)

	E-W	N-S
Base shear [kN]	5830	7537
Base shear [Weight][1]	0.23W	0.30W
Roof displacement [m][2]	0.133	0.082
Roof drift [Height][3]	0.0037H	0.0023H

[1] Weight above foundation W= 25195 kN [2] Displacement relative to base [3] Height above foundation H=36.4m

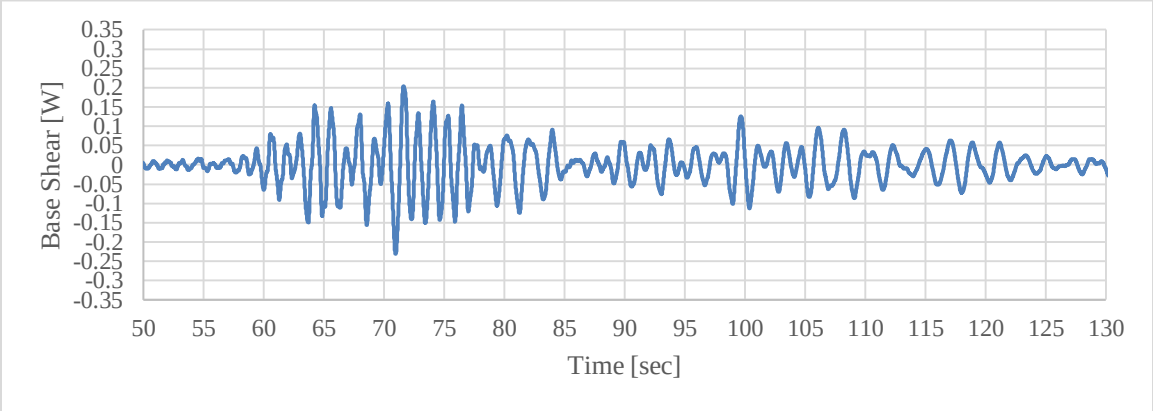

Figure 5.5: CO56 analysis: base shear vs. time E-W direction (peak: 71s)

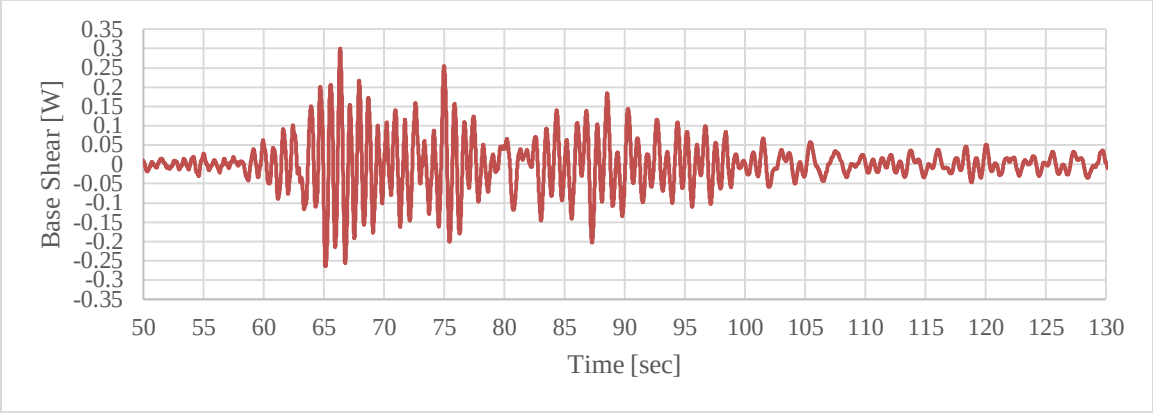

Figure 5.6: CO56 analysis: base shear vs. time N-S direction (peak: 66.4s)

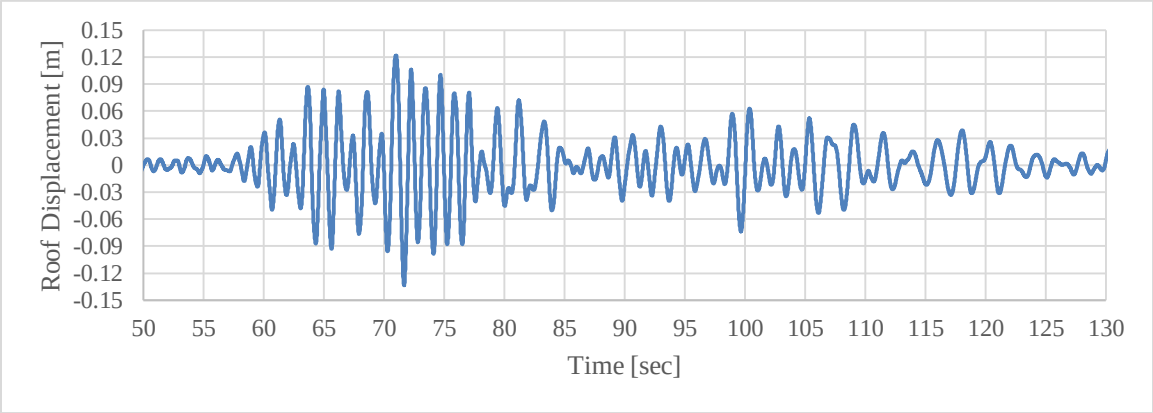

Figure 5.7: CO56 analysis: roof displacement vs. time E-W direction (peak: 71.7s)

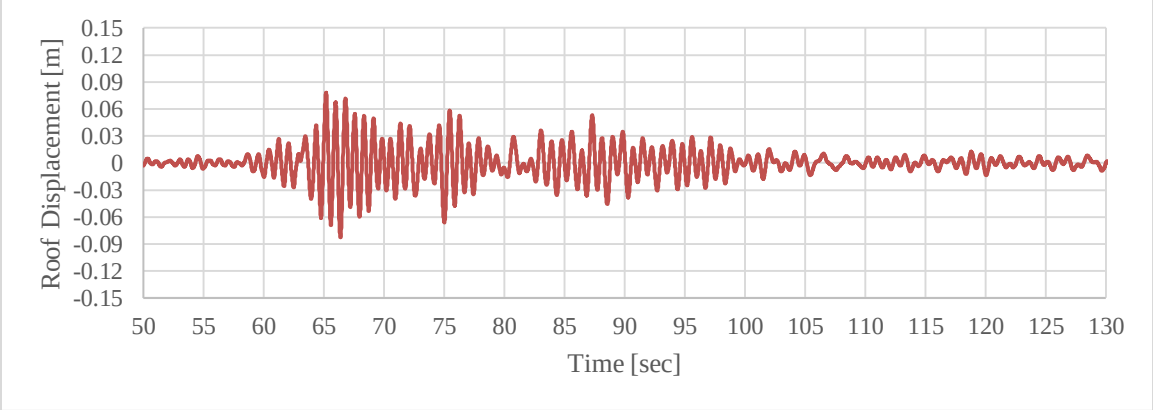

Figure 5.8: CO56 analysis: roof displacement vs. time N-S direction (peak: 66.4s)

To further confirm the effectiveness of the retrofit two additional parameters were analyzed: one at a system level and the other at a local level. For the system level, the proportion of lateral forces carried by RC Frames 1 and 5 and those carried by the steel braced frames were defined. At a local level, the forces resisted by elements damaged by the earthquake of 1979 are compared to their theoretical capacities. The later will also serve to verify the linear elastic assumption.

In Table 5.4 we can see most of the lateral forces (82%) are resisted by the steel frames in both façades reducing to less than 2% the demand in the exterior frames, which suffered the most damage in 1979. These results are also consistent with the design assumption by Del Valle mentioned in previous chapters, which indicated that the retrofit was designed to resist the entirety of the seismic loads.

Table 5.4: Lateral forces resisted by façade frames (CO56) (1 kN = 0.225 kip, 1 m = 39.37 in)

Frame	Shear [kN]	% Base Shear
Frame 1 Steel	2393	41%
Frame 1 RC	53	1%
Frame 5 RC	96	1.6%
Frame 5 Steel	2418	41%

For the local assessment, element capacities were computed according to the provisions of ACI 318. Shear capacity was computed using the following equations (in SI units):

$$Vn = Vc + Vs \quad (Eq\ 5.1)$$

$$Vc = 0.17\sqrt{f'c}\, b_w d \quad (Eq\ 5.2)$$

$$Vs = \frac{A_v f_y d}{S} \quad (Eq\ 5.3)$$

where $f'c$ is the concrete compressive strength in MPa, b_w is the web width in mm (average depth was used for deep beam), and d is the distance from the extreme compression fiber to the longitudinal tension reinforcement in mm, A_v is the area of shear reinforcement within a distance S and f_y is the yield strength of the shear reinforcement. This results in the spandrel having a shear capacity of 455 kN. The shear capacity for each of the columns is indicated in Table 5.7.

Additionally, the first yield moments for the spandrels and demand/capacity ratios for columns was automatically computed in SAP2000 based on section properties. The first yield moment for the spandrels is 628 kN-m and is consistent through the floor levels being analyzed. Tables 5.5 through 5.7 presents the results of this element-level analysis.

Table 5.5: Capacity analysis of spandrels (CO56) (1 kN = 0.225 kip, 1 kN-m = 0.738kip-in)

Spandrel Capacity Analysis					
Frame	Level	Shear [kN]	Demand/capacity ratio[1]	Moment [kN-m]	Demand/yield ratio[2]
1	1	156	**34%**	343	**55%**
1	2	126	**28%**	455	**72%**
1	3	123	**27%**	440	**70%**
5	1	137	**30%**	377	**60%**
5	2	121	**27%**	441	**70%**
5	3	120	**26%**	431	**69%**

1 Compared to a shear capacity of 455 kN

2 Compared to a first yield moment of 628 kN-m

Table 5.6: P-M-M demand/capacity analysis of columns (CO56) (1 kN = 0.225kip, 1 kN-m = 0.738 kip-in)

Column	Level	Axial [kN]		Moment E-W [kN-m]	Moment N-S [kN-m]	Demand/capacity ratio
		Max.	Min.			
A1	PB	1416	1416	114	82	**49%**
A1	1	1047	1047	96	180	**46%**
A1	2	721	721	100	143	**42%**
A1	3	454	454	89	133	**36%**
C1	PB	909	909	107	84	**53%**
C1	1	558	558	89	160	**48%**
C1	2	285	285	97	139	**43%**
C1	3	145	145	90	122	**36%**
A5	PB	1655	1655	101	187	**44%**
A5	1	1223	1223	87	155	**38%**
A5	2	846	846	91	140	**36%**
A5	3	540	540	82	129	**31%**
C5	PB	1449	1449	105	171	**49%**
C5	1	1102	1102	88	163	**44%**
C5	2	775	775	93	141	**39%**
C5	3	493	493	84	124	**33%**

Table 5.7: Shear capacity analysis of columns (CO56) (1 kN = 0.225 kip, 1 kN-m = 0.738 kip-in)

Column	Level	Shear capacity [kN]	Shear demand [kN]	Demand/capacity ratio
A1	PB	346	60	**17%**
A1	1	337	181	**54%**
A1	2	328	161	**49%**
A1	3	319	148	**46%**
C1	PB	346	59	**17%**
C1	1	337	165	**49%**
C1	2	328	145	**44%**
C1	3	319	127	**40%**
A5	PB	346	121	**35%**
A5	1	337	160	**48%**
A5	2	328	162	**49%**
A5	3	319	143	**45%**
C5	PB	346	117	**34%**
C5	1	337	160	**48%**
C5	2	328	150	**46%**
C5	3	319	127	**40%**

The results of the tables clearly show how all critical columns are working below 55% of their shear capacity while spandrels use less than a third of their shear capacity and reach 72% of the yielding moment. The evidence mentioned above suggests that the linear elastic assumption with cracked sections resembles the actual behavior of the building and that the retrofit provided good performance.

5.2.2: TH Analysis: Station CO56 Ground Motion Record from September 19th, 2017 without Soil-Structure Interaction

The second time-history analysis was run using the fixed base instead of the calibrated soil-structure interaction. This with the intention to assess the extent of the effects of the soil-structure interaction in the seismic behavior of the building, given its significant effect on the modal properties of the building.

The results of the time history analysis show a clear difference between the fixed base and SSI models (Table 5.8 and Figures 5.9 through 5.12). As indicated by the modal analysis, the fundamental periods of the structure are reduced up to 50% when using a fixed base. The transverse (E-W) maximum base shear caused by the 2017 CO56 motion increases by 6% while the longitudinal (N-S) is reduced by 60%. This is due to an increase in 20% in the spectral acceleration for the first traverse mode (E-W) and a decrease of 51% in the longitudinal one (N-S).

The combination of the increase in stiffness and the reduction of forces results in a decrease of the N-S roof displacements of 87% for the fixed base model. In the other direction, the increase of lateral forces is clearly counteracted by the increase of stiffness and results in a reduction of 44% of the displacements. Such difference illustrates the impact of the soil-structure interaction in the displacements of the structure.

Table 5.8: SSI vs. fixed base time-history analysis results (1 kN =0 .225 kip, 1 m = 39.37 in)

	E-W			N-S		
	SSI	Fixed	Difference	SSI	Fixed	Difference
Natural period [sec]	1.23	0.85	-31%	0.84	0.43	-49%
Spectral acceleration Sa [g]	0.25	0.30	20%	0.37	0.18	-51%
Base shear [kN]	5830	6154	6%	7537	3068	-59%
Base shear [Weight][1]	0.23W	0.24W		0.30W	0.12W	
Roof displacement [m][2]	0.133	0.075	-44%	0.082	0.010	-87%
Roof drift [Height][3]	0.0037H	0.0020H		0.0023H	0.0003H	

[1] Weight above foundation W= 25195 kN [2] Displacement relative to base [3] Height above foundation H=36.4m

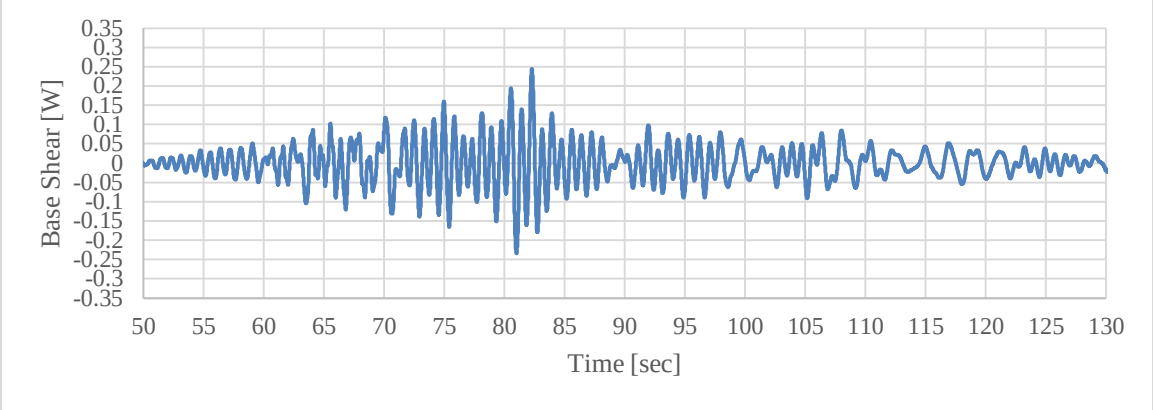

Figure 5.9: CO56 fixed base analysis: base shear vs. time E-W direction (peak: 82.3s)

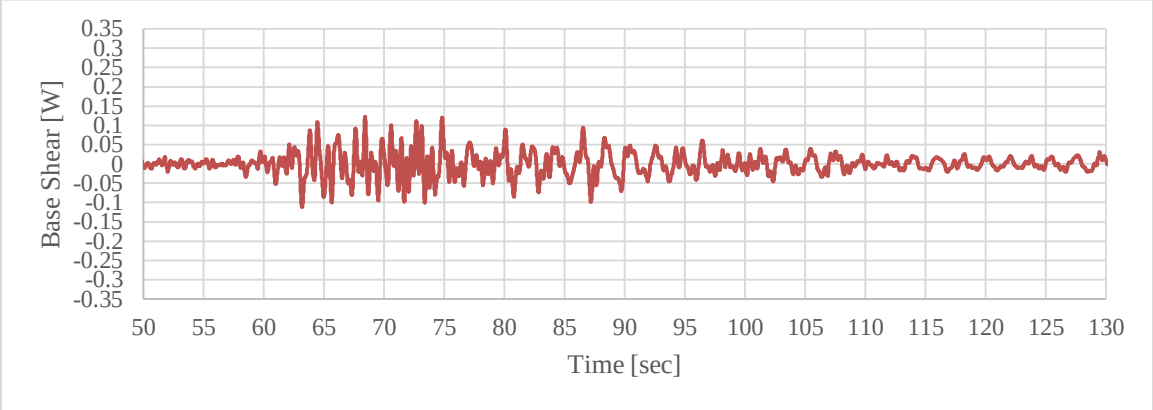

Figure 5.10: CO56 analysis: base shear vs. time N-S direction (peak: 68.4s)

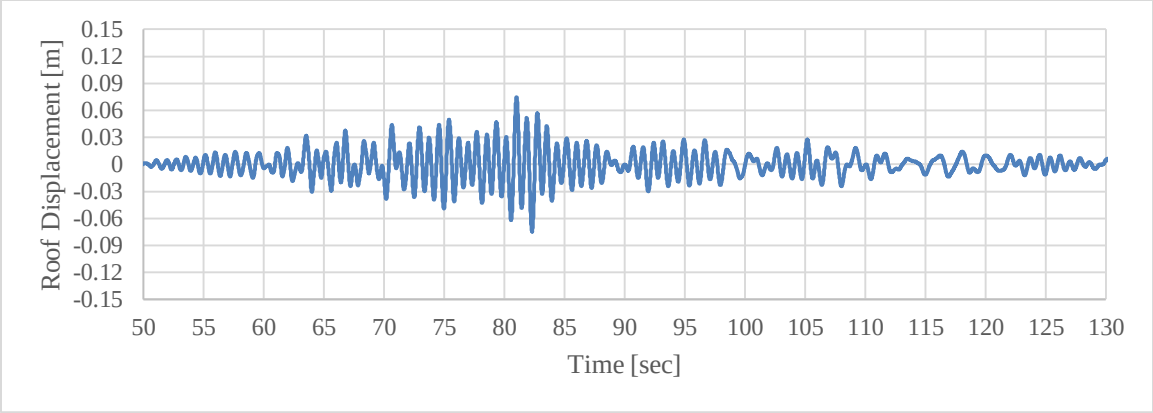

Figure 5.11: CO56 analysis: roof displacement vs. time E-W direction (peak: 81s)

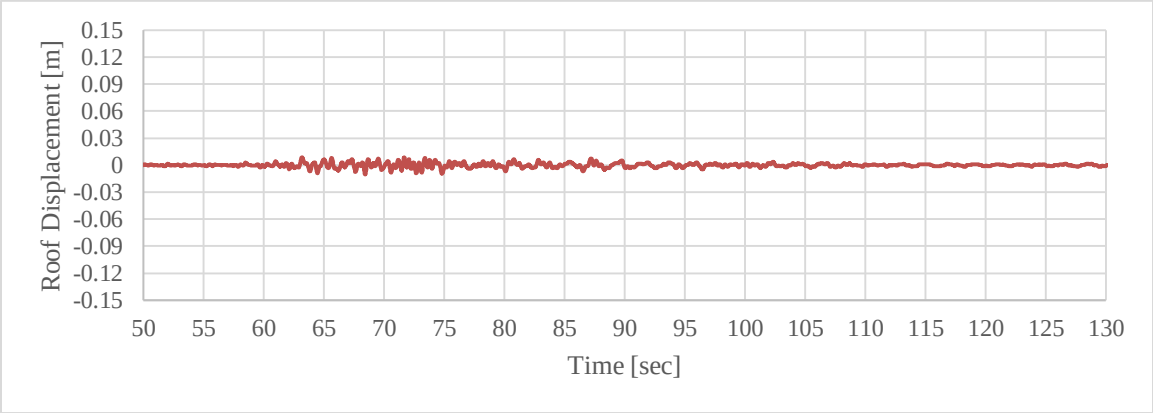

Figure 5.12: CO56 analysis: roof displacement vs. time N-S direction (peak: 68.4s)

Additionally, the proportion of the forces resisted by the steel frame added during the retrofit remains the same at 82% and changes to the demands of critical elements damaged during the 1979 earthquake remain inside the 10% range (Tables 5.9 and 5.10). This value is proportional to the small increase in forces in the E-W direction.

Table 5.9: SSI vs. fixed base spandrel demand/capacity ratio comparison

Frame	Level	Shear demand/capacity ratio			Demand/yield moment ratio		
		SSI	Fixed	difference	SSI	Fixed	difference
1	1	34%	32%	**-2%**	55%	64%	**10%**
1	2	28%	29%	**2%**	72%	81%	**9%**
1	3	27%	28%	**1%**	70%	77%	**7%**
5	1	30%	32%	**2%**	60%	68%	**8%**
5	2	27%	29%	**2%**	70%	80%	**10%**
5	3	26%	28%	**2%**	69%	77%	**8%**
Average				**1%**			**9%**

Table 5.10: SSI vs. fixed base column demand/capacity ratio comparison

Frame	Level	Shear demand/capacity ratio			P-M-M demand/capcity ratio		
		SSI	Fixed	difference	SSI	Fixed	difference
A1	PB	17%	19%	**2%**	49%	39%	**-10%**
A1	1	54%	62%	**8%**	46%	38%	**-8%**
A1	2	49%	53%	**4%**	42%	35%	**-6%**
A1	3	46%	51%	**4%**	36%	31%	**-5%**
C1	PB	17%	20%	**3%**	53%	36%	**-17%**
C1	1	49%	57%	**8%**	48%	34%	**-14%**
C1	2	44%	49%	**5%**	43%	32%	**-11%**
C1	3	40%	47%	**7%**	36%	28%	**-8%**
A5	PB	35%	39%	**4%**	44%	37%	**-6%**
A5	1	48%	55%	**7%**	38%	39%	**1%**
A5	2	49%	56%	**6%**	36%	35%	**-1%**
A5	3	45%	50%	**5%**	31%	31%	**-1%**
C5	PB	34%	34%	**0%**	49%	37%	**-12%**
C5	1	48%	50%	**3%**	44%	38%	**-6%**
C5	2	46%	52%	**7%**	39%	34%	**-5%**
C5	3	40%	46%	**6%**	33%	30%	**-3%**
Average				**5%**			**-7%**

5.2.3: TH Analysis: Station SCT Ground Motion Record from September 19th, 2017

To understand the effects of local soil conditions on the behavior of the structure, an additional analysis with the ground motion record from the SCT station was compared to the results from Section 5.2.1.

The results of the analysis (Table 5.11 and Figures 5.3 through 5.16) show that the local conditions have an effect on the building response, as mentioned in Section 5.1.3. The base shear and displacements are reduced by 15% and 17% respectively in the transverse direction (E-W). On the other direction (N-S) the reduction is even larger with 48% for the base shear and 57% for the displacements. The higher reduction in the N-S direction is directly related to the characteristics of the motion record, as explained in Section 5.1.2.

The difference is notable also considering that both records are from the same seismic event, come from stations with similar local condition (zone IIIb) and the distance between them is ~3km (1.86 miles). Thus, we can confirm that the selection of motion records with local conditions similar to the site of interest is critical to properly simulate the behavior of the structure.

Table 5.11: CO56 (2017) vs. SCT (2017) time-history analysis results (1 kN = 0.225 kip, 1 m = 39.37 in)

	E-W			N-S		
	CO56	SCT	Difference	CO56	SCT	Difference
Base shear [kN]	5830	4949	-15%	7537	3927	-48%
Base shear [Weight][1]	0.23W	0.20W		0.30W	0.16W	
Roof displacement [m][2]	0.133	0.111	-17%	0.082	0.036	-57%
Roof drift [Height][3]	0.0037H	0.0030H		0.0023H	0.0010H	

[1] Weight above foundation W= 25195 kN [2] Displacement relative to base [3] Height above foundation H=36.4m

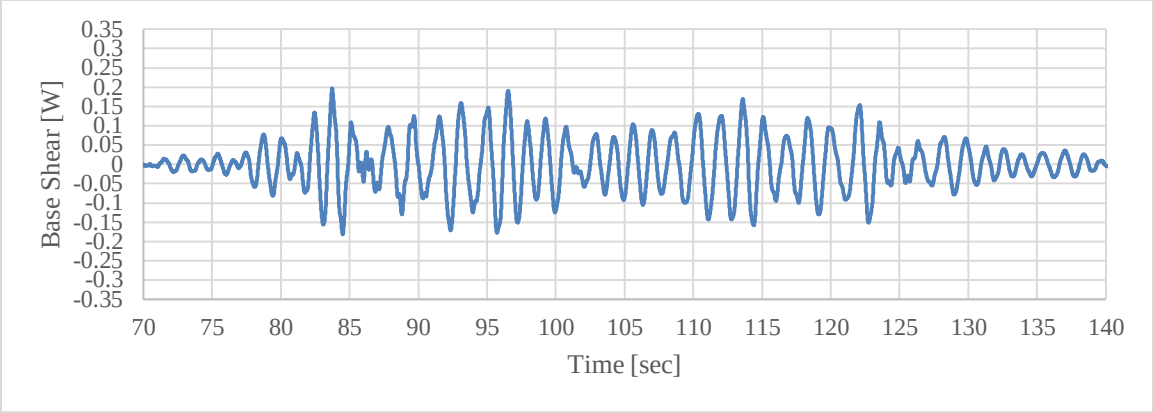

Figure 5.13: SCT 2017 analysis: base shear vs. time E-W direction (peak: 83.7s)

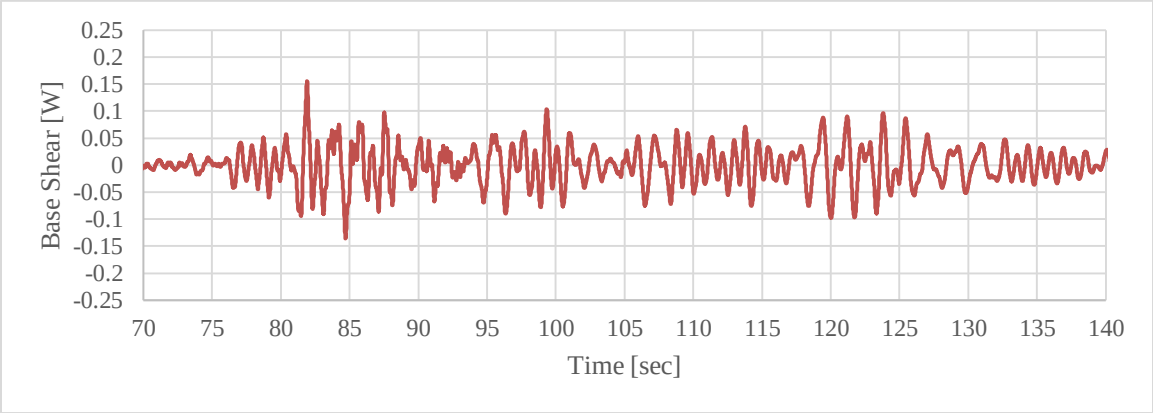

Figure 5.14: SCT 2017 analysis: base shear vs. time N-S direction (peak: 81.9s)

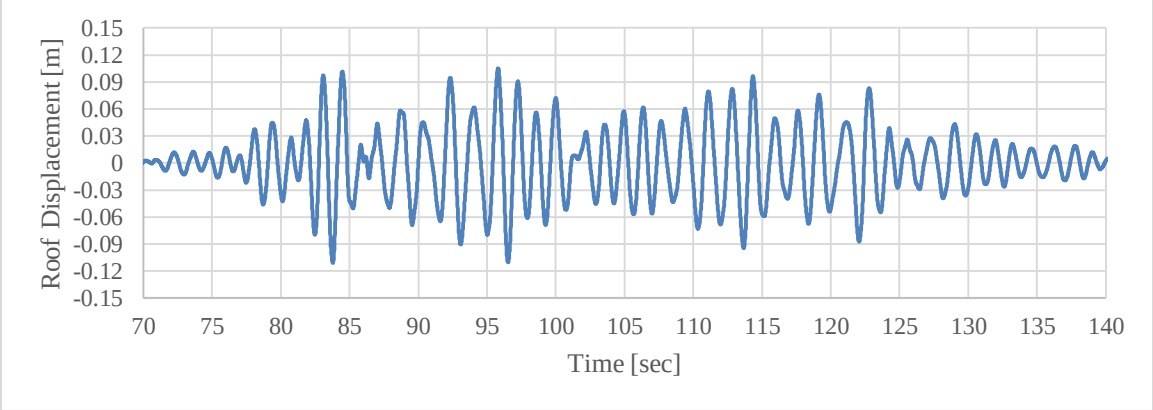

Figure 5.15: SCT 2017 analysis: roof displacement vs. time E-W direction (peak: 83.8s)

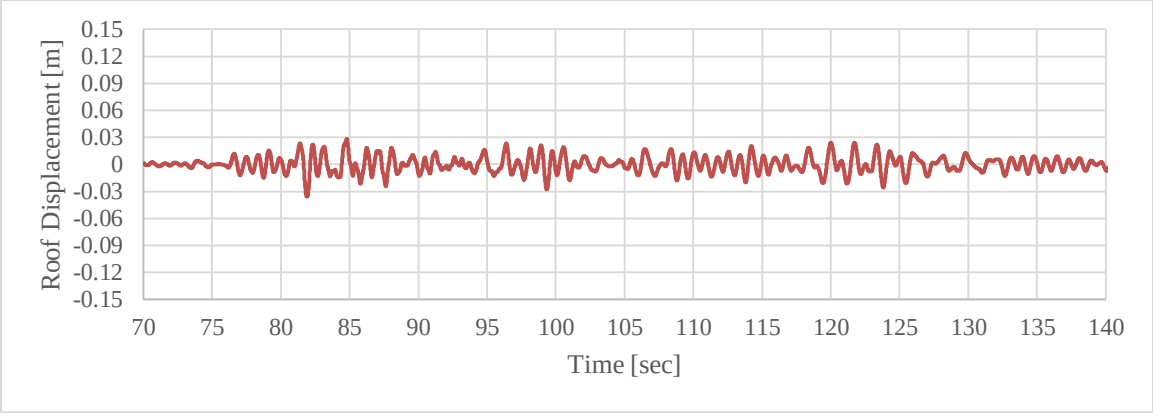

Figure 5.16: SCT 2017 analysis: roof displacement vs. time N-S direction (peak: 81.9s)

Another parameter analyzed was the proportion of the base shear resisted by the steel frame, which for the third time remained approximately 82% of the total. This proves that this proportion is mainly linked to the building characteristics.

Finally, the information regarding the local demand/capacity ratio in the previously damaged elements (Tables 5.12 and 5.13) shows a reduction of 5% in the spandrels with a higher reduction of 10% in the columns. The reason for this difference is the slight reduction force demands in both directions, with the spandrel affected only by the reduction in the E-W forces while the column benefits from both E-W and N-S reductions.

Table 5.12: CO56 (2017) vs. SCT (2017) spandrel demand/capacity ratio comparison

Frame	Level	Shear demand/capacity ratio			Demand/yield moment ratio		
		CO56	SCT	difference	CO56	SCT	difference
1	1	34%	29%	**-5%**	55%	53%	**-2%**
1	2	28%	25%	**-2%**	72%	65%	**-7%**
1	3	27%	25%	**-3%**	70%	62%	**-8%**
5	1	30%	30%	**0%**	60%	55%	**-5%**
5	2	27%	26%	**-1%**	70%	66%	**-5%**
5	3	26%	25%	**-1%**	69%	63%	**-6%**
Average				**-2%**			**-5%**

Table 5.13: CO56 (2017) vs. SCT (2017) column demand/capacity ratio comparison

Frame	Level	Shear demand/capacity ratio			P-M-M demand/capcity ratio		
		CO56	SCT	difference	CO56	SCT	difference
A1	PB	17%	16%	**-2%**	49%	37%	**-12%**
A1	1	54%	50%	**-4%**	46%	35%	**-11%**
A1	2	49%	43%	**-6%**	42%	33%	**-9%**
A1	3	46%	41%	**-6%**	36%	28%	**-8%**
C1	PB	17%	16%	**-1%**	53%	37%	**-16%**
C1	1	49%	44%	**-5%**	48%	34%	**-14%**
C1	2	44%	38%	**-6%**	43%	32%	**-11%**
C1	3	40%	35%	**-4%**	36%	28%	**-8%**
A5	PB	35%	35%	**0%**	44%	33%	**-11%**
A5	1	48%	43%	**-4%**	38%	33%	**-6%**
A5	2	49%	47%	**-3%**	36%	30%	**-6%**
A5	3	45%	40%	**-5%**	31%	26%	**-5%**
C5	PB	34%	28%	**-6%**	49%	36%	**-13%**
C5	1	48%	40%	**-8%**	44%	34%	**-10%**
C5	2	46%	41%	**-4%**	39%	31%	**-8%**
C5	3	40%	35%	**-5%**	33%	27%	**-6%**
Average				**-4%**			**-10%**

5.2.4: TH Analysis: Station SCT Ground Motion Record from September 19th, 1985

Finally, a time-history dynamic analysis was conducted with the SCT record from the 1985 earthquake. As mentioned in the previous section, the data obtained from this analysis should be used for a qualitative analysis given the lack of more accurate information. However, the information can still provide an approximate comparison between the responses to the 1985 and 2017 events.

The results (Table 5.14 and Figures 5.17 through 5.20) demonstrate the different characteristics of the 1985 earthquake compared to the 2017 event. Regarding the N-S direction, we have a reduction of 51% in the base shear and 57% in the roof displacement for 1985. In the E-W there is an increase in the base shear of 14%, meaning that this analysis presents the highest value overall. However, the displacement remains the same most likely due to the characteristics of the motion.

Table 5.14: CO56 (2017) vs. SCT (1985) time-history results (1 kN = 0.225 kip, 1 m = 39.37 in)

	E-W			N-S		
	CO56	SCT 85	Difference	CO56	SCT 85	Difference
Base shear [kN]	5830	6655	14%	7537	3661	-51%
Base shear [Weight][1]	0.23W	0.26W		0.30W	0.15W	
Roof displacement [m][2]	0.133	0.132	-1%	0.082	0.034	-59%
Roof drift [Height][3]	0.0037H	0.0036H		0.0023H	0.0009H	

[1] Weight above foundation W= 25195 kN [2] Displacement relative to base [3] Height above foundation H=36.4m

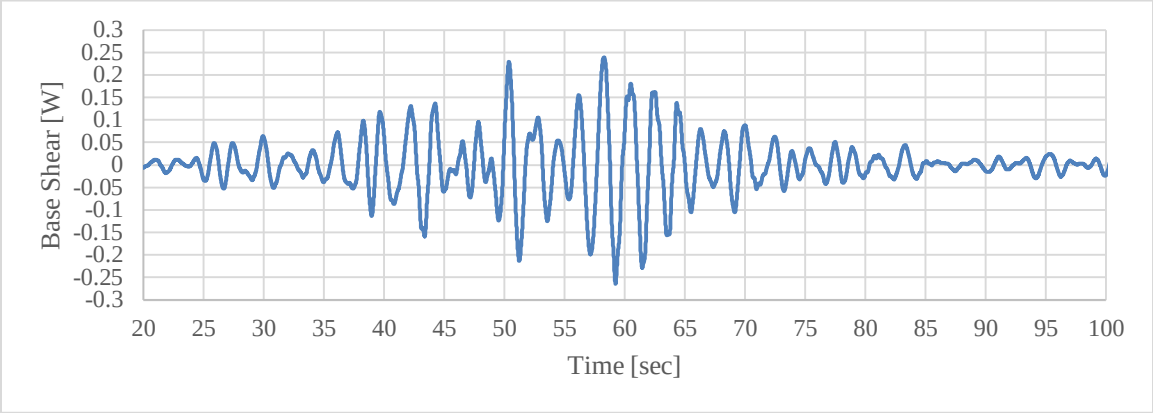

Figure 5.17: SCT 1985 analysis: base shear vs. time E-W direction (peak: 59.3s)

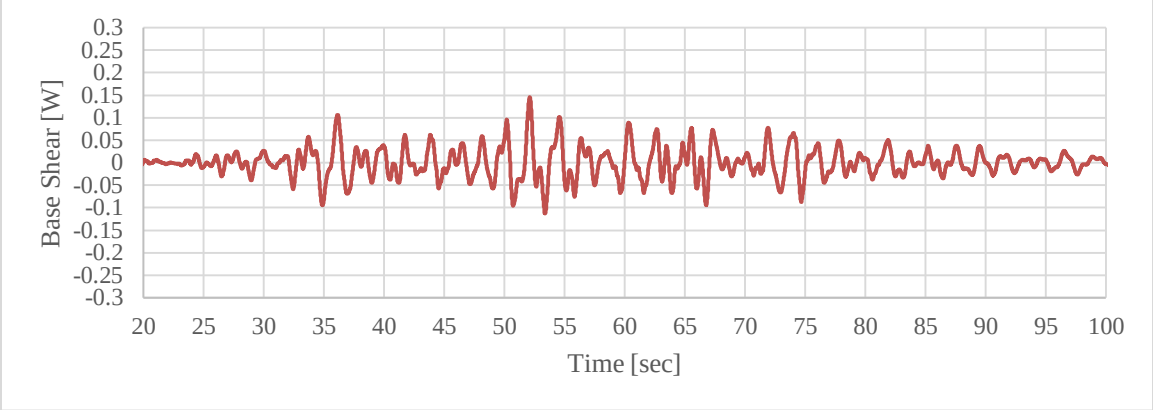

Figure 5.18: SCT 1985 analysis: base shear vs. time N-S direction (peak: 52.1s)

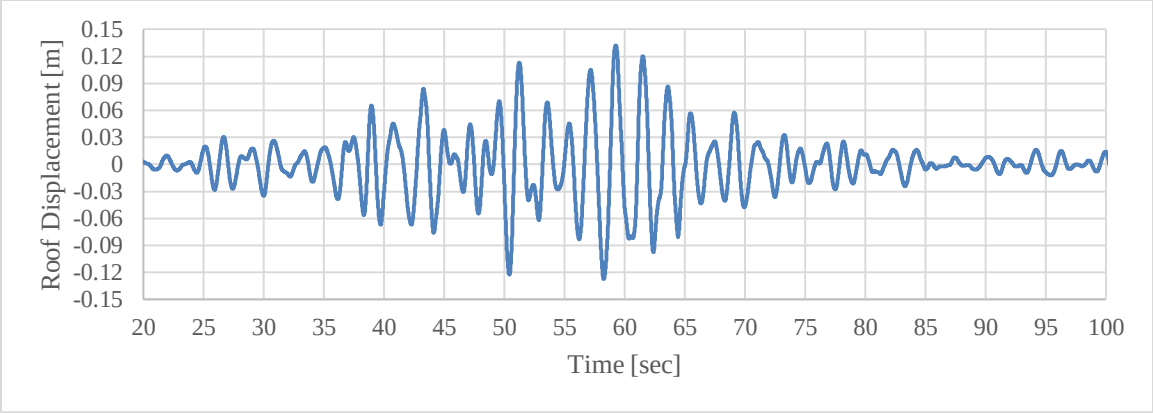

Figure 5.19: SCT 1985 analysis: roof displacement vs. time E-W direction (peak: 59.3s)

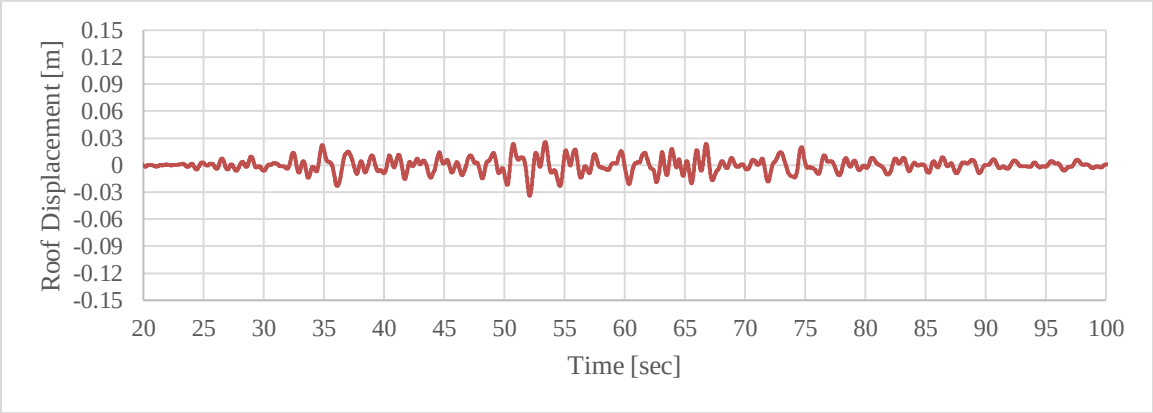

Figure 5.20: SCT 1985 analysis: roof displacement vs. time N-S direction (peak: 52.1s)

Even with an increase in base shear in the E-W direction, the ratios in the previously damaged elements barely change except for the column P-M-M interaction (Tables 5.15 and 5.16). The more pronounced change in column ratios (-%10) is most likely due to the reduction in moment demand in the N-S direction, which has no direct effect in the spandrels. These minimum changes support the idea that the 1985 EQ had an effect of the same magnitude but with different punctual characteristics.

Table 5.15: CO56 (2017) vs. SCT (1985) spandrel demand/capacity ratio comparison

Frame	Level	Shear demand/capacity ratio			Demand/yield moment ratio		
		CO56	SCT 85	difference	CO56	SCT 85	difference
1	1	34%	33%	**-2%**	55%	61%	**6%**
1	2	28%	28%	**0%**	72%	74%	**2%**
1	3	27%	26%	**-1%**	70%	69%	**-1%**
5	1	30%	33%	**3%**	60%	62%	**2%**
5	2	27%	28%	**1%**	70%	73%	**3%**
5	3	26%	26%	**0%**	69%	69%	**0%**
Average				**0%**			**2%**

Table 5.16: CO56 (2017) vs. SCT (1985) column demand/capacity ratio comparison

Frame	Level	Shear demand/capacity ratio			P-M-M demand/capcity ratio		
		CO56	SCT 85	difference	CO56	SCT 85	difference
A1	PB	17%	18%	**1%**	49%	38%	**-11%**
A1	1	54%	56%	**3%**	46%	36%	**-10%**
A1	2	49%	48%	**-1%**	42%	34%	**-8%**
A1	3	46%	45%	**-2%**	36%	29%	**-6%**
C1	PB	17%	18%	**1%**	53%	34%	**-19%**
C1	1	49%	58%	**9%**	48%	33%	**-15%**
C1	2	44%	47%	**3%**	43%	31%	**-12%**
C1	3	40%	44%	**4%**	36%	27%	**-9%**
A5	PB	35%	37%	**2%**	44%	36%	**-7%**
A5	1	48%	49%	**2%**	38%	36%	**-2%**
A5	2	49%	51%	**1%**	36%	33%	**-3%**
A5	3	45%	44%	**-1%**	31%	29%	**-2%**
C5	PB	34%	35%	**2%**	49%	33%	**-16%**
C5	1	48%	50%	**3%**	44%	35%	**-9%**
C5	2	46%	50%	**5%**	39%	33%	**-6%**
C5	3	40%	42%	**2%**	33%	29%	**-4%**
Average				**2%**			**-9%**

5.3: SUMMARY OF BUILDING RESPONSE

The main findings of the time-history dynamic analyses presented in this chapter are summarized as follows:

1. The characteristics of the motion record have a major role in the forces and the displacements presented by the building during a seismic event. Even two records from the same event and soil classification can result in significant differences in terms of building response. The local soil conditions of Mexico City further intensify the discrepancies.
2. Soil-structure interaction has a major role in structural behavior, both in terms of force and displacement demands. This is due to two different reasons: the additional flexibility of the building and modification of the seismic demands.
3. According to the analytical results, the Durango building was subjected to significant force demands during the 2017 earthquake, with maximum base shears of 0.23*W* in the E-W direction and 0.30*W* in the N-S direction. The 1985 demands have been estimated to be similar or lower than those in 2017.
4. The magnitude of the forces presented by critical elements in the E-W direction shows that the assumption of a linear elastic behavior during the 1985 and 2017 events is correct, validating the information obtained from the analyses.
5. The addition of the steel frame during the retrofit was crucial for the good performance presented by the building during the events analyzed, resisting most of the lateral forces. Given the higher intensity of the 1985 and 2017

events as compared to that of 1979, it is likely that the building would have suffered major damage had it not been retrofitted.

Chapter 6: Conclusions and Recommendations for Future Research

6.1: CONCLUSIONS

Several conclusions are drawn from the seismic analysis conducted on the Durango building. They are summarized as follows:

- Visual inspection proved to be a critical step for the early assessment of the building and the definition of the preliminary assumptions during the development of the analytical model. For example, this initial step shaped two important constraints: the linear elastic behavior during the events of 1985 and 2017 given the lack of apparent structural damage, and the magnitude of the superimposed loads which can be highly variable.
- The most time-consuming and delicate aspect of this type of assessments is the development and calibration of a reliable analytical model. The two parameters with a major effect on the behavior of the model were the soil-structure interaction and geometry of elements in the original and retrofitted structure. Concrete stiffness can be used for fine calibration after the rest of the parameters are established while joint stiffness and superimposed loads can be considered minor players. The final Durango model was able to keep the fundamental modes in the E-W and N-S direction and in torsion in a range of ±5% of the experimental data.
- The ratio between the 2^{nd} and 1^{st} vibration frequencies in a given direction reveals important information about the building dynamic response and can be used for model calibration purposes. A low ratio indicates the building response resembles that of an idealized flexural beam, while a high ratio indicates the response is more like a shear beam. In the calibrated model, the ratios fell low

by 17% at 3.48 in the E-W direction and 27% at 3.09 in the N-S direction, indicating an intermediate type of behavior.

- The adequate modeling of the soil-structure interaction (SSI) is crucial for the accurate simulation of the building characteristics, modifying not only the overall stiffness and displacements by a factor of two, but also the ratios between first and second vibration modes that, as indicated above, are a good indicator of the type of building behavior.
- When conducting a time-history dynamic analysis, the selection of an adequate ground motion record is imperative. The differences caused by local conditions between two records of the same earthquake can introduce significant differences in terms of forces and displacements.
- According to the time-history dynamic analysis, the Durango building was subjected to significant force demands during the 2017 earthquake, with maximum base shears of 0.23W in the E-W direction and 0.30W in the N-S direction. The 1985 demands have been estimated to be similar or lower than those in 2017.
- Through the demand/capacity ratios of critical elements, obtained in the time-history dynamic analyses, it is confirmed the assumption of the linear elastic behavior of the structure during the 2017 event and most likely in 1985. This was verified by checking the forces induced to critical spandrels and columns damaged during the 1979 earthquake. These forces reached less than 80% of the yielding moments in the spandrels, while columns did not reach more than 60% of the ultimate capacity. Shear forces were below 35% of the capacity in the spandrels (using simplified ACI formula) and 60% in the columns.

- The proportion of the base shear resisted by the steel frame in the E-W direction confirms the effectiveness of the retrofit. The maximum shear forces carried by the steel frame remained at 82% of the total base shear through all the different time-history analysis.

6.2: RECOMMENDED FUTURE WORK

The following recommendations are made to further study the behavior of the Durango building:

- The development of nonlinear models of the original and retrofitted building would add the capabilities to simulate damage to the structure under greater demands which could be useful to predict the structural limitations. This additional model could also analyze in depth the interaction between the original structure and the added retrofit, including possible vulnerabilities in the connections.
- During the process of completing the present study, the building foundation was being retrofitted with control piles to correct the leaning of 23.1cm (~9.1in) identified after the 2017 earthquake. Another ambient vibration test is planned after this new intervention is completed to identify possible variations in the soil-structure interaction and overall dynamic properties of the building. Thus, it would be interesting to update the model and conduct new analyses when new vibration data is available. This would allow a comparison of the response for three different configurations of the building.

REFERENCES

Aire, C. & Murià-Vila, 1993. *Evaluación de las propiedades mecánicas de los concretos de un edificio de 14 pisos,* Mexico City: Instituto de Ingenieria UNAM.

American Concrete Institute (ACI), 2014. *Building Code Requirements for Structural Concrete (ACI 318-14),* Farmington Hills, Michigan: American Concrete Institute (ACI).

Arias, J. G., 2005. *Ensayos en Mesa Vibradora de un Modelo a Escala 1:2 de Edificio de Mampoteria Confinada de Tres Niveles,* Mexico City: UNAM.

ATLATD, 2019. *All Things Living All Things Dead: Lake Texcoco.* [Online]
Available at: http://www.allthingslivingallthingsdead.com/cartography
[Accessed 14 August 2019].

BBC, 2017. *Terremoto de 1985: el devastador sismo que cambió para siempre el rostro de Ciudad de México.* [Online]
Available at:
https://www.bbc.com/mundo/noticias/2015/09/150917_mexico_sismo_antes_despues_fotos_an
[Accessed 14 August 2019].

Chopra, A. K., 2012. *Dynamics of Structures.* 4th ed. Berkeley: Pearson.

Computers and Structures, Inc., 2017. *SAP2000,* New York: Computers and Structures, Inc.

Del Valle, E., 1980. Some Lessons From the March 14, 1979 Earthquake in Mexico City. *Proceedings of 7WCEE,* 4(1), pp. 545-552.

Downs, R. E., Hjelmstad, K. D. & Foutch, D. A., 1991. *Evaluation of Two RC Buildings Retrofit with Steel Bracing,* Urbana, Illinois: Department of Civil Engineering University of Illinois at Urbana-Champaign.

El Pais, 1979. *Violento terremoto en México.* [Online]
Available at: https://elpais.com/diario/1979/03/15/internacional/290300404_850215.html
[Accessed 14 August 2019].

Foutch, D. A. et al., 1989. Case Studies of Seismic Strengthening for Two Buildings in Mexico City. *Earthquake Spectra,* Vol. 5(No. 1), pp. 153-174.

Gobierno de la Ciudad de Mexico, 1976. *Nuevo Reglamento de Construcciones,* Mexico City: Editorial Libros Economicos.

IBEROMX, 2017. *14 de marzo de 1979: El sismo que marcó la historia de la IBERO.* [Online]
Available at: https://ibero.mx/prensa/14-de-marzo-de-1979-el-sismo-que-marco-la-historia-de-la-ibero
[Accessed 14 August 2019].

Mendoza, L., Reyes, A. & Luco, J. E., 1991. Ambient Vibration Tests of the Mexicali General Hospital. *Earthquake Spectra,* Vol. 7(No. 2), pp. 281-300.

NTC 2004, 2004. *Normas Tecnicas Complementarias para Diseño y Construccion,* Mexico City: Gobierno de la Ciudad de Mexico.

NTC 2017, 2017. *Normas Tecnicas Complementarias para Diseño y Construccion,* Mexico City: Gobierno de la Ciudad de Mexico.

The Huffpost, 2017. *FOTOS: El antes y después de los edificios derrumbados en CDMX*. [Online]
Available at: http://www.huffingtonpost.com.mx/2017/09/23/fotos-el-antes-y-despues-de-los-edificiosderrumbados-
[Accessed 26 September 2017].